

**ELECTROCHEMICAL DETERMINATION OF PH  
USING PAPER-BASED DEVICES**

by  
**Armelle Metangmo**

**A Thesis**

*Submitted to the Faculty of Purdue University  
In Partial Fulfillment of the Requirements for the degree of*

**Master of Science**



Department of Chemistry & Chemical Biology

Indianapolis, Indiana

August 2019

**THE PURDUE UNIVERSITY GRADUATE SCHOOL**  
**STATEMENT OF COMMITTEE APPROVAL**

Dr. Frédérique Deiss, Chair

Department of Chemistry & Chemical Biology

Dr. John Goodpaster

Department of Chemistry & Chemical Biology

Dr. Eric Long

Department of Chemistry & Chemical Biology

**Approved by:**

Dr. Eric Long

Head of the Graduate Program

*For my family*

## ACKNOWLEDGMENTS

I would like to sincerely thank my advisor, Dr. Frédérique Deiss, for all her support, patience, care and guidance throughout the course of my undergraduate and graduate career. I would like to thank Violet Goodpaster who worked alongside me to finalize this project. I would also like to thank the members of the Deiss Research Lab for their encouragements, friendship and support along the way. I would like to thank Boris for the support, patience, love and understanding he showed me during this journey. Lastly, I would like to thank my family, especially my mother for always pushing me to work hard and to never give up.

## TABLE OF CONTENTS

LIST OF TABLES .....	7
LIST OF FIGURES .....	8
ABSTRACT .....	10
CHAPTER 1. INTRODUCTION .....	11
CHAPTER 2. LITERATURE REVIEW .....	12
2.1 Defining pH .....	12
2.2 pH Measurement Methods .....	13
2.2.1 Commercial pH Measurement Methods .....	14
2.3 Current Research on pH Measurement .....	15
2.3.1 Flexible Devices for Measuring pH .....	16
2.4 Conclusion .....	18
CHAPTER 3. EXPERIMENTAL SECTION .....	19
3.1 Material and Regents .....	19
3.2 Solutions Preparation .....	19
3.3 Fabrication of Paper-based Devices .....	20
3.4 Electrochemical Measurements .....	20
3.5 Washing Procedure for Devices .....	20
3.6 Sodium Carbonate Treatment .....	21
3.7 Plasma Treatment .....	21
CHAPTER 4. ELECTROCHEMICAL PAPER-BASED PH SENSOR: PROOF OF CONCEPT .....	22
4.1 pH Sensing Method via Quinone Oxo-group .....	23
4.2 Fabrication of pH Sensor .....	25
4.3 Proof of Concept .....	28
4.3.1 Unpolished vs. Polished Paper-based Devices .....	28
4.3.2 Unpolished PBD: Testing Different Buffers .....	30
4.3.3 Data Analysis: Software vs. Manual Peak Picking .....	31
4.3.4 Assessment and Problems Encountered .....	32
4.4 Conclusion .....	34

CHAPTER 5. MODIFICATION OF PAPER-BASED DEVICES TO IMPROVE REDOX PEAKS .....	36
5.1 Sodium Carbonate Treated Paper-based Devices .....	36
5.2 Square Wave Voltammetry (SWV) .....	37
5.3 Plasma Treatment.....	39
5.3.1 Oxygen Plasma Treatment using Air.....	39
5.3.2 Oxygen Plasma Treatment using Pure Oxygen.....	43
5.3.3 Effect of Plasma on Reference Electrode .....	45
5.4 Conclusion .....	47
CHAPTER 6. CHANGES TO THE DESIGN OF DEVICE AND CONDITIONING STEP...	48
6.1 Change in Design: Filter Paper .....	48
6.2 Change in Design: Area of Working Electrodes.....	50
6.3 Optimization of the Method: Conditioning Step .....	52
6.4 Conclusion .....	53
CHAPTER 7. DETERMINATION OF PH WITH OPTIMIZED DEVICE AND METHOD..	54
7.1 Measuring pH in Various Buffers and Solutions.....	54
7.2 Effect of Adding Sodium Chloride to pH Solutions.....	57
7.3 Measuring pH from 0 to 13.....	58
7.3.1 HCl/NaOH .....	58
7.3.2 Standard pH Solutions .....	58
7.4 Repeatability of Method on PBDs .....	59
7.5 pH Measurement of Artificial saliva.....	60
7.6 Conclusion .....	61
CHAPTER 8. FUTURE WORK.....	63
8.1 Preliminary Work on Identifying the pH-sensing Species .....	63
8.2 Real Samples of Food and Beverages.....	65
8.3 Apply PBD pH Sensor to Real Saliva and Bacteria .....	66
CONCLUSION.....	67
REFERENCES .....	68

## LIST OF TABLES

Table 1. a) Flow rate of air treatment, b) Flow rate of pure oxygen treatment.....	21
Table 2. List of buffer solutions and pH range. ....	54
Table 3. Composition list for artificial saliva .....	61
Table 4. List of quinone derivatives and their associated reduction reactions. ....	63

## LIST OF FIGURES

Figure 1. Universal pH scale.....	13
Figure 2. Conventional pH meters .....	14
Figure 3. Schematic diagram of ISFET .....	16
Figure 4. Scheme of the graphite layers on an edge plane pyrolytic electrode .....	24
Figure 5. Fabrication of electrochemical paper-based device .....	27
Figure 6. a) Photograph of a polishing pad. b) Paper-based device before and after polishing. c) Overlay of CVs for the unpolished device.....	28
Figure 7. Cyclic voltammograms showing the shift of redox potential as pH increases.....	29
Figure 8. a) CV overlay of McIlvaine buffers and NaOH/HCl solutions, b) Calibration curve for the potentials of cathodic peaks .....	30
Figure 9. a) CV overlay of phosphate buffer. b) Calibration curve for the potentials of cathodic peaks done over the average of two cycles for each pH. ....	31
Figure 10. a) Calibration plot of peak values collected manually from excel b) calibration plot of values collected using the software eL-Chem viewer.....	32
Figure 11. Assessment of method to measure pH on PBDs.. .....	33
Figure 12. a) CV of McIlvaine buffer at pH 3, noisy peaks b) CV of phosphate buffer at pH 5, peaks not visible.....	34
Figure 13. a) Overlay of CVs collected using sodium-carbonate-modified PBD, solutions of 0.1 M phosphate buffer. b) Calibration curve of the oxidation potential peaks. c) Calibration curve of the reduction potential peaks. ....	37
Figure 14. a) Square Wave Voltammograms of sodium carbonate pretreated device. b) Calibration curve of SWV peaks. ....	38
Figure 15. a) CVs of an oxygen plasma treated paper-based device. b) Calibration curve of the oxidation peaks. c) Calibration curve of the reduction peaks .....	40
Figure 16. a) CVs of an oxygen plasma treated paper-based device. b) Calibration curve of the oxidation peaks. c) Calibration curve of the reduction peaks. ....	41
Figure 17. a-b) Overlay of CVs of phosphate and McIlvaine buffers using the same plasma-treated device. c) Overlay of CVs of phosphate buffer on another plasma-treated device. ....	42
Figure 18. a) Overlay of CVs of different devices used to screen for the device with well-defined redox peaks. b) CV overlay of pure oxygen plasma treated device. c) Calibration curve of oxidation peaks. d) Calibration curve of reduction peaks.....	44
Figure 19. a) Overlay of SWV collected in different phosphate buffers with pH values ranging from 5 to 9. b) Calibration curve of potential peaks. ....	45



Figure 20. CVs collected before and after plasma treatment to demonstrate the increase in capacitive current.....	45
Figure 21. a) Paper-based devices before plasma, b) after plasma, and c) after the reference electrode is cut and replaced. d) CVs of Oxygen plasma treated device.....	47
Figure 22. Comparison between different pore-size filter papers.....	48
Figure 23. Calibration plot for smaller pore-size filter paper. ....	50
Figure 24. a-d) Photographs of devices with varying area of WE. e) CVs. f) Calibration curve of oxidation peaks. g) Calibration curve of reduction peaks.....	51
Figure 25. CVs starting with different starting potential.. ....	52
Figure 26. a) Overlay of Citrate buffer. b) Calibration curve of reduction peaks potential over the average of two cycles.....	55
Figure 27. a) Calibration curves of HCl/NaOH solutions, citrate buffers, McIlvaine buffers, and phosphate buffers tested on device A. b) Calibration curves of same solutions tested on device B. ....	56
Figure 28. Overlay of plots with and without NaCl.....	57
Figure 29. Calibration curve of potentials of the reduction peaks for pH ranging from 1 to 13. .	58
Figure 30. Plots of potentials of the reduction peaks versus pH on the PBD in standard pH solutions .....	59
Figure 31. Repeatability tests on four different PBDs performed by two users. ....	60
Figure 32. Calibration curve the potential of reduction peaks of two devices in artificial saliva. 61	
Figure 33. CVs of 9,10-Phenanthrenequinine (PAQ), Tetrachloro-o-Benzoquinone (TCBQ) and 1,4-Benzoquinone (p-Ben).....	64
Figure 34. CVs of Catechol .....	65
Figure 35. CV overlay of distilled white vinegar .....	66

## ABSTRACT

Author: Metangmo, Armelle. MS

Institution: Purdue University

Degree Received: August 2019

Title: Electrochemical Determination of pH using Paper-based Devices

Committee Chair: Frédérique Deiss

For the past decade, many microfluidic paper-based analytical devices have been developed and used in different research fields. These devices are low-cost, portable, flexible, sterilizable, disposable, and easy to manufacture. The microfluidic paper-based analytical devices offer good alternatives to measurements and assays commonly performed in laboratories for analytical and clinical purposes, especially in diagnostics. In this work, we developed an electrochemical paper-based pH sensor. The determination of pH is essential in applications in areas as diverse as in the food industry, agriculture, health care or water treatment. The method presented in this work is an electroanalytical method that involves quantification of pH using stencil-painted graphite electrodes. Preliminary tests showed that pH can be determined on paper-based devices, thus indicating the presence of electroactive elements sensitive to pH on the surface of our electrodes (Chapter 4). Chemical modification of the electrode by adsorption with sodium carbonate and modification of the surface of the electrode was accomplished via: oxygen (ambient air) plasma treatment and pure oxygen plasma treatment. These treatments were to attempt to improve the definition of redox peaks on the CVs (Chapter 5). The changes made to the design of the paper-based device and the addition of a conditioning step improved the definition of the redox peaks on the CVs and increased the pH-sensing ability of our method (Chapter 6). The pH-sensing ability of our method was evaluated by testing solutions over a wide pH range. Adding sodium chloride to samples adjust the solution for accurate pH determination. The pH was successfully measured for solutions with values ranging from 1 to 13 and for artificial saliva samples prepared with pH values in the cavity-prone range (Chapter 7). This work offers a method that uses electroactive elements sensitive to pH on the surface of the PBD electrodes for pH-sensing.

## CHAPTER 1. INTRODUCTION

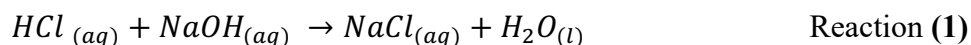
The research presented in this thesis describes the development of an electrochemical microfluidic paper-based analytical device for pH-sensing. Chapter 2 describes the importance of pH and provides examples of techniques used to measure pH. In Chapter 4, preliminary tests on the electrochemical microfluidic paper-based analytical devices demonstrate the feasibility of pH measurements. Chapter 5 describes three different approaches for modification of the surface of the electrodes painted on the paper-based devices: sodium carbonate, plasma treatment with air, and pure oxygen plasma treatment. Chapter 6 describes changes made to the design of the paper-based devices and the addition of a conditioning step to improve the definition of redox peaks and improve the precision of the method for measuring pH. In Chapter 7, the optimized paper-based device and method are applied to measure the pH of various solutions pH ranging from 1 to 13.

This project is the first milestone in the development of an electrochemical paper-based device for analyzing the pH in bacterial biofilms formed on teeth (or plaque). Dental caries is one of the most common chronic diseases world-wide. Assessing the pH of the plaque of a patient can indicate the likelihood of cavities and allow to guide the caregiver for providing preventive care. Cariogenic bacteria that lead to dental caries thrive in acidic conditions, this inspired the tests of artificial saliva with different pH that fall in the cavity-prone range done in Chapter 7. Some characteristics and requirements of the current electrochemical pH-sensing paper-based device are linked to these future applications. For example, the need for the device to be flexible, small, disposable, and low-cost. These characteristics would allow for easy and isolated collection of samples (plaque) which would allow for preservation of the main characteristics of the bacterial biofilm. More importantly, we avoid chemical modifications of the sensor with additional chemical reagents that would not be compatible with being in contact with patient's teeth.

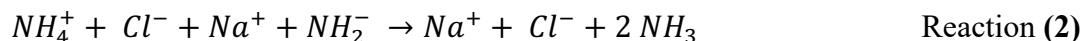
## CHAPTER 2. LITERATURE REVIEW

### 2.1 Defining pH

The determination of pH is a concept that goes as far back as the ancient Greeks (350 BC). Even though the concept of pH was not fully understood, the people were able to distinguish between acid and base by conducting taste tests to determine if a substance was sour (acid) or bitter (base).<sup>1</sup> Substances like vinegar and lemon juice were considered acidic and a mixture of ashes with animal fat to make soap was considered basic. Over the centuries the understanding for the concept of acid-base was developed and later defined by the participation of many chemists: Arrhenius, Brønsted, Lowry, and Lewis.<sup>2</sup> In the early development of the theory of acids and bases the different observations made included: acids tasting sour and bases tasting bitter, the changes in color indicating acid or bases, the reactions between acid and bases to form salts (Miessler & Tarr, 1999, Ch. 6, p. 165).<sup>2</sup> The first to explain the concept of acid-base in molecular terms was Svante Arrhenius in 1880 - 1890. The Arrhenius definition of acids/bases states that acids react in aqueous solutions to form hydrogen ions and bases react in aqueous solutions to form hydroxide ions. The reaction between hydrogen ions and hydroxide ions forms water as seen in reaction 1:



In 1923 Brønsted and Lowry explained the concept for a more general use that includes gases compared to Arrhenius whose definition only referred to aqueous solutions. They defined an acid as a hydrogen ion donor and the base as hydrogen ion acceptor. They also introduced the concept of conjugate acids-bases. An example of the Brønsted and Lowry theory is shown in the reaction of  $NH_4Cl$  and  $NaNH_2$  (Reaction 2):



Net reaction:



$NH_4^+$  is the acid and  $NH_2^-$  is the base which yields two  $NH_3$  molecules as both the conjugate base and conjugate acid. Finally Lewis explained the acid-base theory as: a Lewis acid is an electron-pair acceptor and a Lewis base is an electron-pair donor. (Miessler & Tarr, 1999, Ch. 6, p. 170)<sup>2</sup> Chemical reactions between acids and bases can be used to determine pH, which ranges from pH

0 to 14 (figure 1). The term pH is an acronym for “power of hydrogen” where “p” stands for the negative logarithm and the “H” stands for the concentration of the element hydrogen.<sup>3</sup>

$$pH = -\log [H^+] \quad (\text{eq. 1})$$

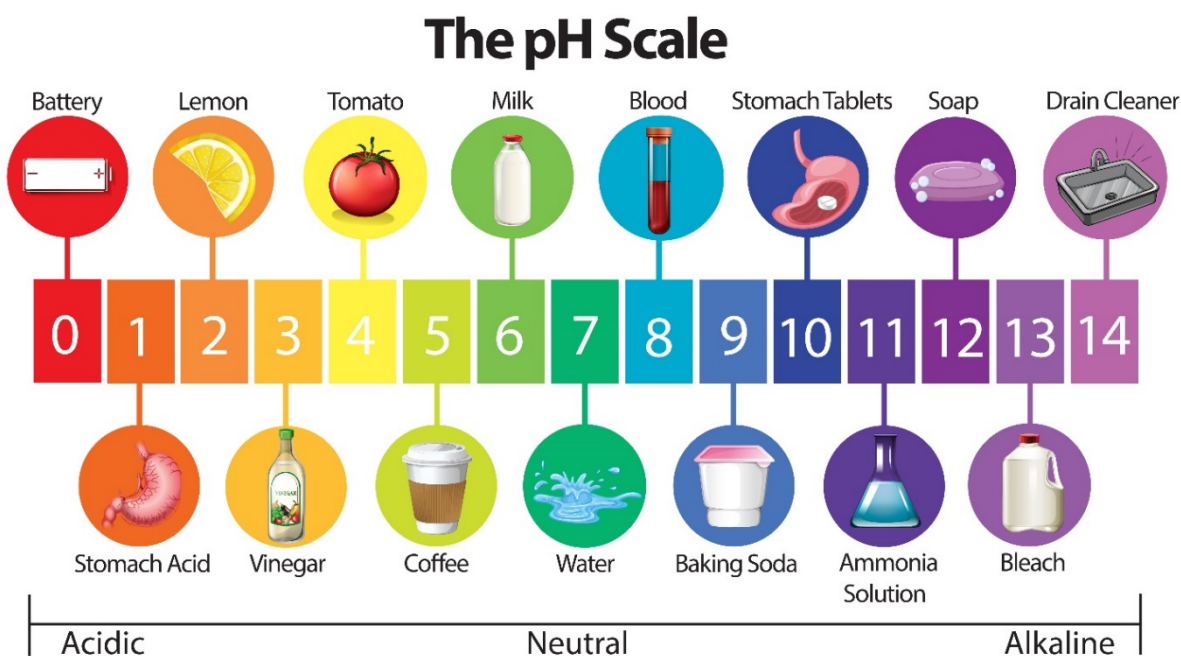


*Figure 1. Universal pH scale.<sup>4</sup>*

## 2.2 pH Measurement Methods

pH measurements are used in areas such as the food industry, medicine, water treatment and biopharmaceutical industries.<sup>3, 5-7</sup> Measuring pH in the food industry is of great importance. It avoids causing health problems to consumers by providing products with well-defined properties such as controlling the pH of milk to avoid sour milk. Controlling the pH is also critical for successful food and beverages preparation, for example when making fruit jelly gels.<sup>8</sup> Measuring pH in the medicine and biopharmaceutical industries is crucial because it is used to understand the nature of chemical processes and to monitor quality and safety for humans.<sup>3</sup>

### 2.2.1 Commercial pH Measurement Methods

Many pH sensors exist for determining pH levels. Common methods to measuring pH include using litmus paper, pH strips, and glass probes. Paper strips perform colorimetric measurement of pH and use a color chart for pH determination. They are less expensive, but are not always precise and thus render quantification difficult compared to glass probes.<sup>3</sup> Examples of glass probes used to measure pH are shown in figure 2. Glass probes rely on potentiometry to measure pH. Potentiometric methods involve the measurement of the potential of an electrochemical cell in the absence or with negligible current flow and no redox reaction occurring. Other instrumental electrochemical methods use potentiometry but also amperometry.<sup>5,7</sup> Amperometric methods involve the measurement of ions in a solution based on current or changes in current while redox reactions occur.



Figure 2. Conventional pH meters.<sup>9-11</sup>

Glass probes have high sensitivity and selectivity.<sup>7</sup> However, glass probes have some limitations, they are fragile,<sup>3</sup> and non-disposable.<sup>12</sup> The electrode also has issues with instability when reading the pH of very basic solutions with values above  $\sim 11$ . The term “alkali error” refers to interference of alkali metals such as  $\text{Na}^+$  and  $\text{K}^+$ , or with very acidic solutions ( $\text{pH} \leq 1$ , “acid error”)<sup>7,8, 12, 13</sup> They also require regular calibration before taking measurements due to instability and drift in potential.<sup>5, 7</sup>

### 2.3 Current Research on pH Measurement

Over the past decades there has been an increase in development of different types of pH sensors; such as optical pH sensors,<sup>3,14-17</sup> ion-sensitive field effect transistor (ISFET),<sup>3, 18, 19</sup> or graphene-based devices.<sup>5, 7, 20-24</sup> Optical pH sensors rely on a sensing platform, pH reagent(s) and a detection method. The reagents in optical sensing consist of absorption or fluorescence-based molecular probes. The properties of these reagents are modified with the change in concentration of the hydrogen ions in the solution.<sup>15, 16</sup> Advantages of optical pH sensors are that they do not require the use of a reference electrode and they have a high sensitivity and specificity.<sup>14, 15</sup> For example, Gotor *et al.* reported the development of seventeen different (2,6-diethyl-1,3,5,7-tetramethyl)-BODIPY dyes to act as pH probes and detect pH ranging from 0 to 14 in aqueous solution.<sup>16</sup> They demonstrated how the fluorescence response can be read by a smartphone application using different illumination sources.<sup>16</sup> Optical pH sensors have some disadvantages, since measuring the pH of a solution is done by detecting changes in optical factors in the solution, the accuracy of the results can be limited by environmental factors such as light conditions, color of the sample, or presence of particulates.<sup>15</sup> Long-term stability of immobilized indicators is also often limited due to photobleaching or leaching of the dyes and dependence to temperature.<sup>14, 17</sup>

In 1970 P. Bergeve was the first to report an ISFET where the current flow is controlled by an electric field.<sup>19, 25</sup> The ISFET has a gate region called insulator that houses the sensing films, ion-selective sensing layers include SiO<sub>2</sub>, Si<sub>3</sub>N<sub>4</sub>, Ta<sub>2</sub>O<sub>5</sub>, Al<sub>2</sub>O<sub>3</sub>.<sup>18, 19, 25</sup> The sensing layer detects a change in the ion concentration of a solution and generates a potential on the gate, and the drain-source current change in the channel is measured (Figure 3).<sup>19, 25</sup> ISFET has been reported to have a linear pH sensitivity of 54.8 mV per pH unit to 48.5mV per pH unit through a pH range of 1 to 12 using a Al<sub>2</sub>O<sub>3</sub>/SiO<sub>2</sub> gate ISFET sensor.<sup>19</sup> ISFET are widely used as pH sensor, and in biomedical areas such as medical diagnostics and pharmaceuticals. In 2002 Choi *et al.* reported an ISFET glucose sensor system with fast recovery by electrolysis.<sup>26</sup> They achieved a recovery time of two minutes using electrolysis compared to 10 or 20 minutes from conventional methods.<sup>26</sup> There are, however, some limitations to the use of an ISFET pH sensor such as amplified noise and poor reproducibility.<sup>3</sup>

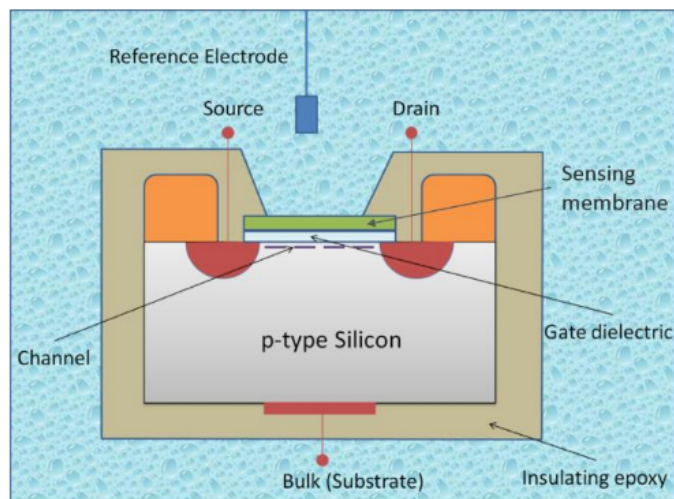


Figure 3. Schematic diagram of ISFET.<sup>25</sup>

Other novel pH sensors based on electrochemical techniques use a pH-dependent analyte or a mediator. The pH-dependent mediator is used to monitor the electrochemical activity as the  $H^+$  concentration changes.<sup>27</sup> There are multiple studies using this approach with the mediator chosen being a polymer film, like polyaniline,<sup>13, 28, 29</sup> or organic redox species.<sup>5, 19, 24</sup>

### 2.3.1 Flexible Devices for Measuring pH

There are many methods and materials used to develop flexible pH sensors. Such sensors exhibit advantages such as being low-cost, portable, sterilizable, noninvasive, wearable, and disposable. The growing interest in the development of such devices is due to their ability to be applied in many fields: they can be used for diagnostics, for pH monitoring in food and water, and can be easily accessible to areas that lack proper infrastructure and laboratories. Most flexible platforms that have been proposed for measuring pH typically rely on electrochemical techniques.<sup>28, 30-35</sup> The fabrication of flexible pH sensors include inkjet ink,<sup>29</sup> screen printing,<sup>22, 27, 28</sup> paper-based,<sup>32, 36</sup> and plastic-based (polyethylene terephthalate (PET)).<sup>30</sup>

Wang *et al.* reported the use of a tattoo-based ion-selective electrodes for non-invasive potentiometric monitoring of epidermal pH levels.<sup>29</sup> Despite the different scenarios (e.g., stationary cycling, no fluid ingested during exercise, abundant sweat) under which the non-invasive electrode was tested the results displayed a Nernstian response.<sup>29</sup> Voltammetric



techniques are commonly characterized by their ability to give a Nernstian response, i.e., to follow the Nernst equation (equation 2) in the conditions of the analysis.<sup>6, 7, 27</sup>

$$E_p = E_{f_{Ox/Red}}^{\circ} - 2.303 \frac{RT}{nF} \log \frac{[Red]}{[Ox]} \quad (\text{eq. 2})$$

where  $E_p$  represents the measured potential,  $E_f^{\circ}$  represents the formal potential,  $n$  represents the number of electrons,  $R$  represents the ideal gas constant,  $T$  represents the temperature, and  $F$  represents the Faraday constant. Wang *et al.* also reported a bandage-based wearable potentiometric sensor for monitoring wound pH.<sup>28</sup> The device is based on the combination of a screen printed sensor and a bandage, which displays selectivity and a Nernstian response over a pH range of 5.5 to 8.<sup>28</sup> Another group, Javey *et al.* reported a wearable and non-invasive electrochemical plastic-based PET device for the simultaneous monitoring of  $\text{Ca}^{2+}$  and pH.<sup>30</sup> The pH of body fluids (sweat, tears, and urine) was accurately measured on the wearable system with integrated circuits and a wireless transceiver as the human body deviated from homeostasis.<sup>30</sup>

For centuries paper has been used as a substrate for chemical analysis.<sup>37</sup> Flexible devices made for analytical purposes with paper-based materials have been extensively studied over the past decade. In 2007 Whitesides *et al.* reported a microfluidics paper-based analytical device fabricated by making a pattern using photolithography on paper.<sup>37, 38</sup> The microfluidics paper-based devices have since been used in multiple applications which include point-of-care (POC) diagnostics and colorimetric detection.<sup>36, 39</sup> Deiss *et al.* developed a flow-through system on paper patterned Teflon to create peptide arrays for cell-based assays. These Teflon arrays caused organic solvents to be confined in a zone on the paper and allowed for flow-through synthesis of 100 peptides.<sup>40</sup> Heat could be applied to enhance the synthetic rate of conversion up to 15 fold.<sup>41</sup> Paper-based devices were also developed for POC culture and colorimetric detection of the antibiotic susceptibility of several strains of bacteria (*Escherichia coli* and *Salmonella typhimurium*).<sup>39</sup> Lopez-Ruiz *et al.* presented a paper-based microfluidics device for colorimetric determination of nitrite concentration and pH.<sup>36</sup> They achieved a resolution of 0.04 units of pH, 0.09 of accuracy, and a mean squared error of 0.167. The limit of detection for nitrite achieved was  $0.52 \text{ mg L}^{-1}$  and a resolution of 0.51% at  $4.0 \text{ mg L}^{-1}$ .<sup>36</sup>

In 2009 Dungchai *et al.* reported the first electrochemical paper-based devices.<sup>42</sup> They screen-printed electrodes on the microfluidics device for quantitative measurement of biomarkers in serum.<sup>42</sup> Some advantages to using electrochemical paper-based devices are portability, low

cost, high sensitivity, and high selectivity. Nie *et al.* reported electrochemical microfluidics-paper-based analytical devices integrated with a commercial glucometer for the quantitative analysis of glucose, cholesterol, lactate, and alcohol in blood or urine.<sup>43</sup> Henry *et al.* also reported the use of a paper-based device for a combined colorimetric and electrochemical quantification of metals (Pb, Cd, Ni, Fe, Cu, and Cr) in environmental samples.<sup>44</sup>

Sensors fabricated using carbon-based material such as carbon nanotubes, glassy carbon and graphite have been studied at length for the past decades.<sup>20-24</sup> Some of the advantages of carbon-based materials are a wide potential range, good conductivity, versatility, availability and low-cost.<sup>6, 7, 21</sup> Dossi *et al.* introduced an electrochemical paper-based device with pencil-drawn (graphite) electrodes for the detection of the separation of ascorbic acid and sunset yellow found in many food. They were able to detect ascorbic acid at concentrations as low as 30  $\mu\text{M}$  and sunset yellow as low as 90  $\mu\text{M}$ .<sup>45</sup> Dossi *et al.* also introduced the use the pencil-drawn electrochemical paper-based device with a dual working electrode for the detection of two solutions with dopamine/ascorbic acid and paracetamol/ascorbic acid.<sup>46</sup>

Carbon-based materials are widely and commonly used in electrochemistry. The surface is known to have functional groups that are naturally present on the surface and easily react with other molecules.<sup>6, 7, 21</sup> The work presented in the four chapters after the experimental section introduces a paper-based platform to measure pH via the redox reaction of oxo-groups at the surface of painted graphite electrodes.

## 2.4 Conclusion

This chapter presented the importance of pH detection, and described different methods employed to measure pH. This chapter described the use of paper-based materials for colorimetric and electrochemical detection and finally described flexible devices and their advantages as pH sensors. Carbon-based material is introduced into the fabrication of the electrochemical paper-based devices, the carbon-based material is used due to its rich chemistry. The next chapter describes all the materials and methods used in this work. The fourth chapter will present the development of our electrochemical paper-based devices for the measurement of pH.

## CHAPTER 3. EXPERIMENTAL SECTION

### 3.1 Material and Regents

Whatman® qualitative filter paper Grade 114, Grade P4 and Grade P2 purchased from Fisher Scientific. Carbon conductive carbon paint supplied by EMS; conductive adhesive 502 supplied by SPI; graphite (E3456) and silver/silver chloride/carbon ink (E2908) conductive ink manufactured by Ercon (Wareham, MA). Sodium Phosphate Monobasic Anhydrous ( $\text{NaH}_2\text{PO}_4$ ), Potassium Chloride (KCl) were purchased from Fisher BioReagents. Sodium Phosphate Dibasic Anhydrous ( $\text{Na}_2\text{HPO}_4$ ), Sodium Hydroxide (NaOH), Sodium Chloride (NaCl), Sodium Bicarbonate ( $\text{NaHCO}_3$ ), Sodium Citrate ( $\text{Na}_3\text{C}_6\text{H}_5\text{O}_7$ ), Potassium Phosphate Monobasic ( $\text{KH}_2\text{PO}_4$ ), Potassium Thiocyanate (KSCN) were purchased from Fisher Scientific. Sodium Carbonate anhydrous, ACS, 99.5% ( $\text{Na}_2\text{CO}_3$ ), Catechol 99% ( $\text{C}_6\text{H}_6\text{O}_2$ ), 9,10-Phenanthrenequinone 95%, p-Benzoquinone 98+% were purchased from Alfa Aesar. Citric Acid ( $\text{C}_6\text{H}_8\text{O}_7$ ), Tetrachloro-o-benzoquinone 97% were purchased from Acros Organics. Buffers for pH Meter (pH 4.0, 7.0, 10.0) were purchased from Mettler Toledo. Standard buffer solutions (pH 1 to 12) were purchased from Sigma Aldrich.

### 3.2 Solutions Preparation

Mcllvaine buffers were prepared by mixing 0.2 M  $\text{Na}_2\text{HPO}_4$  with 0.1 M citric acid in different proportions to adjust pHs. Phosphate buffers were prepared by mixing 0.1 M  $\text{Na}_2\text{HPO}_4$  with 0.1 M  $\text{NaH}_2\text{PO}_4$  in different proportions to adjust pHs. Citrate buffers were prepared by mixing 0.1 M citric acid in 0.1 M KCl with 0.1 M sodium citrate in 0.1 M KCl in different proportions to adjust pHs. HCl/NaOH solutions were prepared by mixing 0.1 M HCl with 1 M NaOH in different proportions to adjust pHs. All the powder reagents were weighed on a Mettler Toledo XPE105 analytical balance with antistatic module. The solutions were diluted in volumetric flasks. The pH of the solutions were measured using a Mettler Toledo Sven Compact modular pH meter/ion sensor. The pH meter was calibrated using Mettler Toledo buffer solutions of  $\text{pH } 4.00 \pm 0.02$ ,  $7.00 \pm 0.02$ ,  $10.00 \pm 0.02$  at 25 °C. Artificial saliva (pH 7.85) was prepared using the composition listed in table 3 (AFNOR standard: S90-701).<sup>12,47</sup> 1 M HCl and 1 M NaOH were used to adjust artificial saliva to the desired pH (pH range 3 to 8).

### 3.3 Fabrication of Paper-based Devices

Using Whatman® qualitative filter paper Grade P2 a pattern designed using the graphical software Adobe Illustrator is printed with a XeroxColorQube 8570DN printer and heated in an oven at 150 °C for 2 min to melt the wax and allow it to wick through the thickness of the paper forming hydrophobic walls (wax-patterned microfluidics devices). Using Adobe Illustrator the pattern of the electrochemical cell is designed. The design of the electrodes is cut on a piece of stencil paper using a laser cutter (a Universal Laser System 2.30 CO<sub>2</sub> laser cutter). The backing from the stencil is removed and pressed on the wax-patterned microfluidics devices. Using the conductive ink graphite for the working and counter electrodes (E3456) and silver/silver chloride/carbon ink (E2908) for the pseudo-reference electrode the electrodes are painted on. The stencil is then removed and the devices left to dry for a few hours until the solvent of the paint is fully evaporated. The final product is shown in figure 5d.

### 3.4 Electrochemical Measurements

The cyclic voltammetry (CV) and square wave voltammetry (SWV) were carried out using an Autolab PGstat204 potentiostat with Electrochemical Impedance Spectroscopy FRA2 module for preliminary test and a PGSTAT128 potentiostat with FRA2 module and fast scan voltammetry SCAN250 module for all other tests. Typical potential range for CVs was from 0.5 V to – 0.5 V vs Ag/AgCl/C at a scan rate of 50 mV/s and for SWV was from 0.5 V to – 0.5 V vs Ag/AgCl/C, the frequency of 3 Hz, and the amplitude of 200 mV unless otherwise indicated. For example, when using the conditioning step typical potential range starts from 1V.

### 3.5 Washing Procedure for Devices

Each electrochemical paper-based device was dipped in water for one or two minutes and then air-dry before the first use. After each CV, the PBD was rinsed according to the following procedure. Each side of the device is rinsed three times with milli-Q water from a squirt bottle to remove all the excess solution. The device is then placed in a small beaker containing about 5 mL of milli-Q water for 30 sec. This last step is repeated a second time with fresh milli-Q water. Finally, the device is placed on a clean piece of paper towel and allowed to air-dry before the next use.

### 3.6 Sodium Carbonate Treatment

The electrochemical paper-based device is dipped into a solution of 1 M sodium carbonate overnight (18 h or more). The device is removed from the solution, rinsed using milli-Q water and allowed to dry for over 30 minutes.

### 3.7 Plasma Treatment

We performed plasma treatment on the paper-based devices using a Harrick PDC-001 plasma cleaner with an Agilent IDP-3 dry scroll vacuum pump and a PDC-FMG PlasmaFlo Gas Mixer for accurate control of the gas flowrate and monitoring of the vacuum pressure. The PBD is placed in the plasma cleaner and the chamber is closed, and the vacuum pump is turned on to evacuate the air in the chamber and the pressure is monitored on the PlasmaFlo Gas Mixer. Once the pressure is around 0.145 torr, the 3-way valve is open to allow air to enter the chamber at 0 psig with the flow rate selected from table 1a. The RF is set to HI until we observe a purple-pink glow in the chamber (plasma), the plasma is left on for 3 minutes. After 3 minutes the RF is turned off, the 3-way valve is closed, the plasma cleaner is turned off and the sample is removed. The plasma treatment with pure oxygen follows the same procedure as with the air with the following changes: after the PBD is placed in the chamber and is pumped to 0.145 torr, the 3-way valve that is connected to cylinder of pure compressed oxygen gas is open to allow for oxygen to enter the chamber at 10 psig with the flow rate selected from table 1b.

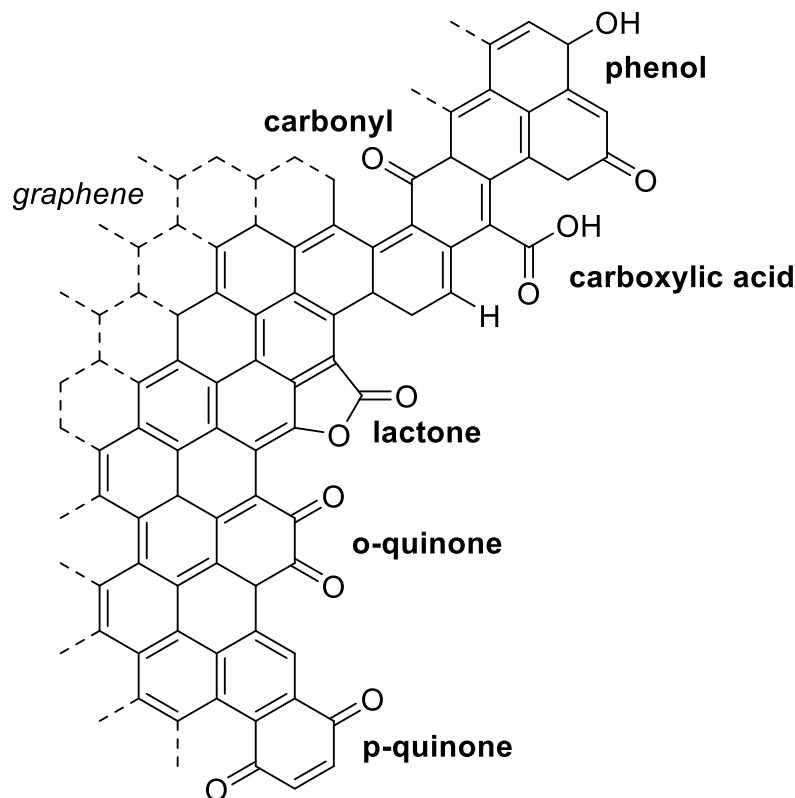
*Table 1. a) Flow rate of air treatment, b) Flow rate of pure oxygen treatment.*

a)	Scale Reading (mm)	Air 0 psig flow (ml/min)	b)	Scale Reading (mm)	Air 10 psig flow (ml/min)
	40	22.9		25	18.3
	45	27.9		30	22.5
	50	32.7		35	27
				40	34.2

## **CHAPTER 4. ELECTROCHEMICAL PAPER-BASED PH SENSOR: PROOF OF CONCEPT**

The detection of pH is important to a large variety of applications, which include pharmaceutical, water treatment, food industry, agriculture, and diagnostics. As described in the second chapter glass probes are the most common method for detection of pH. Despite its high sensitivity and selectivity, the glass probe does have some disadvantages: they are fragile, non-disposable and require regular calibration before taking measurements due to instability and drift in potential. Chapter 2 also presented different pH sensors based on electrochemical techniques and electroactive probes or mediators.

In literature a common redox species used for the detection of pH is quinone moieties as its reduction is pH dependent.<sup>6,27</sup> The formation of oxo-groups on the surface of carbon material are natural occurring when oxygen is present. Other pH sensors involve modification of the electrode where quinone functional groups are attached onto the surface of the electrode.<sup>5, 27, 48</sup> Depending on the carbon-based material used, different functional groups can be formed.<sup>49</sup> Scheme 1 shows examples of various functional groups that form on the surface of carbon material.<sup>6, 21</sup> The functional groups includes oxo-groups such as carboxyl, hydroxyl, ketone, lactone, ether and quinones or hydroquinones.



*Scheme 1. Various functional groups present on graphene surface, adapted from ref 7.*

#### 4.1 pH Sensing Method via Quinone Oxo-group

In this chapter, we describe the fabrication of an electrochemical paper-based device (PBD) developed for the measurement of pH. The pH-sensing relies on the reduction of a functional group, which we believe is quinone (see Chapter 8: Future work for more detail). To explain the concept of pH sensing we based the development of the PBD on previous reports of surface oxo-groups on specific highly treated carbon-based electrodes. Compton *et al.*<sup>7</sup> developed a pH sensor using an Edge Plane Pyrolytic Graphite (EPPG) electrode. Figure 4 depicts ordered graphite layers that are placed parallel to the surface and have a spacing of 3.35 Å between layers. The spacing expose the steps of the edges of the graphite layers which lead to defect sites.<sup>49</sup> The defect sites on the surface of the EPPG electrode react with the oxygen from the air to form a variety of oxo-groups.<sup>7</sup> The functional groups are represented in scheme 1. They reported the determination of pH based on the reduction of the surface quinones; by polishing the EPPG electrode to expose more defect sites which react with oxygen from the air and form more functional groups. The functional groups

formed on the surface of the electrode allowed them to achieved a linear correlation over the aqueous pH range 1.0 to 13.1 with a Nernstian response that corresponds to a two electron, two proton system.<sup>7</sup> Building on this work, Compton *et al.* also reported similar work on glassy carbon electrodes (GCE): by polishing a GCE to a mirror-like surface, it displayed analogous behavior to the EPPG electrodes with a shift of reduction peak potentials correlated to pH values.<sup>6</sup>

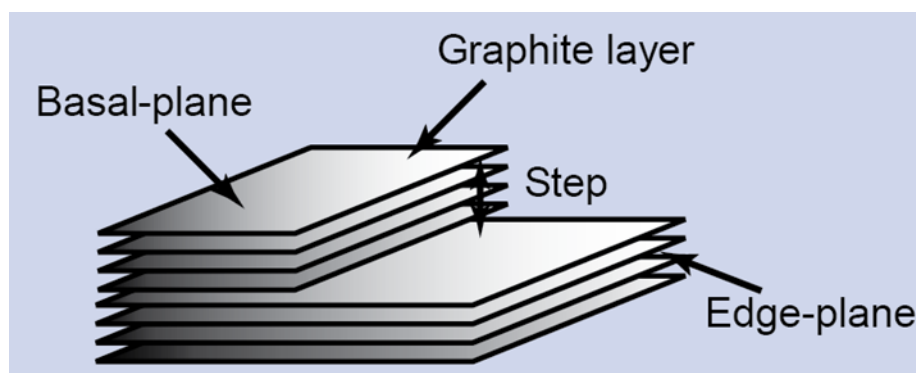
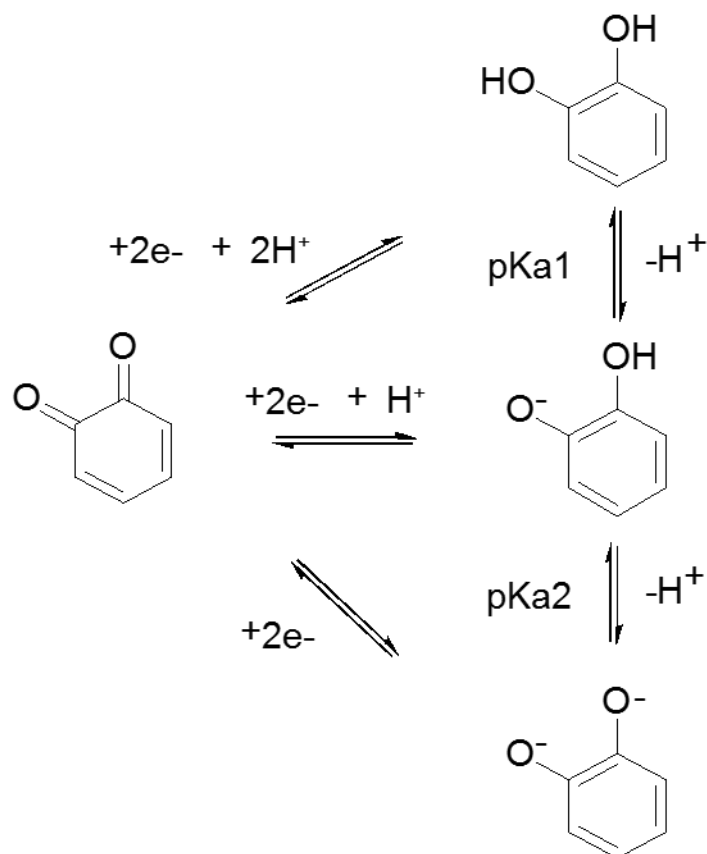


Figure 4. Scheme of the graphite layers on an edge plane pyrolytic electrode.

The possible pathways involved in the reduction of *ortho*-benzoquinone are given in scheme 2. In a study to determine the distribution between *ortho* and *para*-quinone, Schreurs *et al.* found that *ortho*-quinone were the groups that were predominantly formed.<sup>50</sup> The formation of *ortho*-quinone which happens on the same armchair surface of graphite was found to be energetically favorable.<sup>21</sup> *Ortho*-benzoquinone has pKa values of 9.25 and 13.0 in solution at room temperature.<sup>51</sup> The number of two proton/ two electron system associated with the redox process for *ortho*-quinone could give rise to calibration plot with pH range from 1.0 to 13.0.





*Scheme 2. Scheme showing 3 pathways that an ortho-quinone molecule can be reduced following a  $2 H^+/2 e^-$  process.<sup>7</sup>*

#### 4.2 Fabrication of pH Sensor

We selected paper as a substrate for our devices as paper-based devices (PBD) have advantages such as: being low-cost, flexible, portable, sterilizable and disposable. These paper-based devices are made using carbon material with advantages previously listed, namely: low cost, good conductivity and versatile chemistry, which we exploit in this project. The fabrication of the device comprises two parts, the first part is to generate the microfluidic pattern in the paper-based device. The second part is to add the “electrochemical” components to our devices, aka the painted electrodes.

The microfluidic paper-based device is fabricated through the following steps. A pattern forming the hydrophobic and hydrophilic zone shown in figure 5a is printed on a sheet of P2 grade filter paper using a solid-ink wax printer. The paper is then placed in an oven at 150 °C for two

minutes. This step melts the wax and allow for it to wick through the thickness of the paper to form the hydrophobic walls.

To render our paper-based devices “electrochemical”, we add electrodes to the microfluidic paper-based device through the following steps: (i) The electrodes were designed using the graphical software Adobe illustrator, (ii) then a plastic stencil was cut out following the design using a CO<sub>2</sub> laser cutter (Figure 5b). (iii) The stencil is placed over the wax-patterned microfluidics devices for the electrodes to be painted with conductive inks (Figure 5c). Graphite ink is used for the working (WE) and counter (CE) electrodes and silver/silver chloride/carbon ink for the pseudo-reference (RE) electrode. (iv) Once the stencil removed, the paper-based devices are allowed to dry for a few hours until the solvent of the paint is fully evaporated. (v) The devices are then cut into individual devices, the final product (figure 5d), and stored until use.

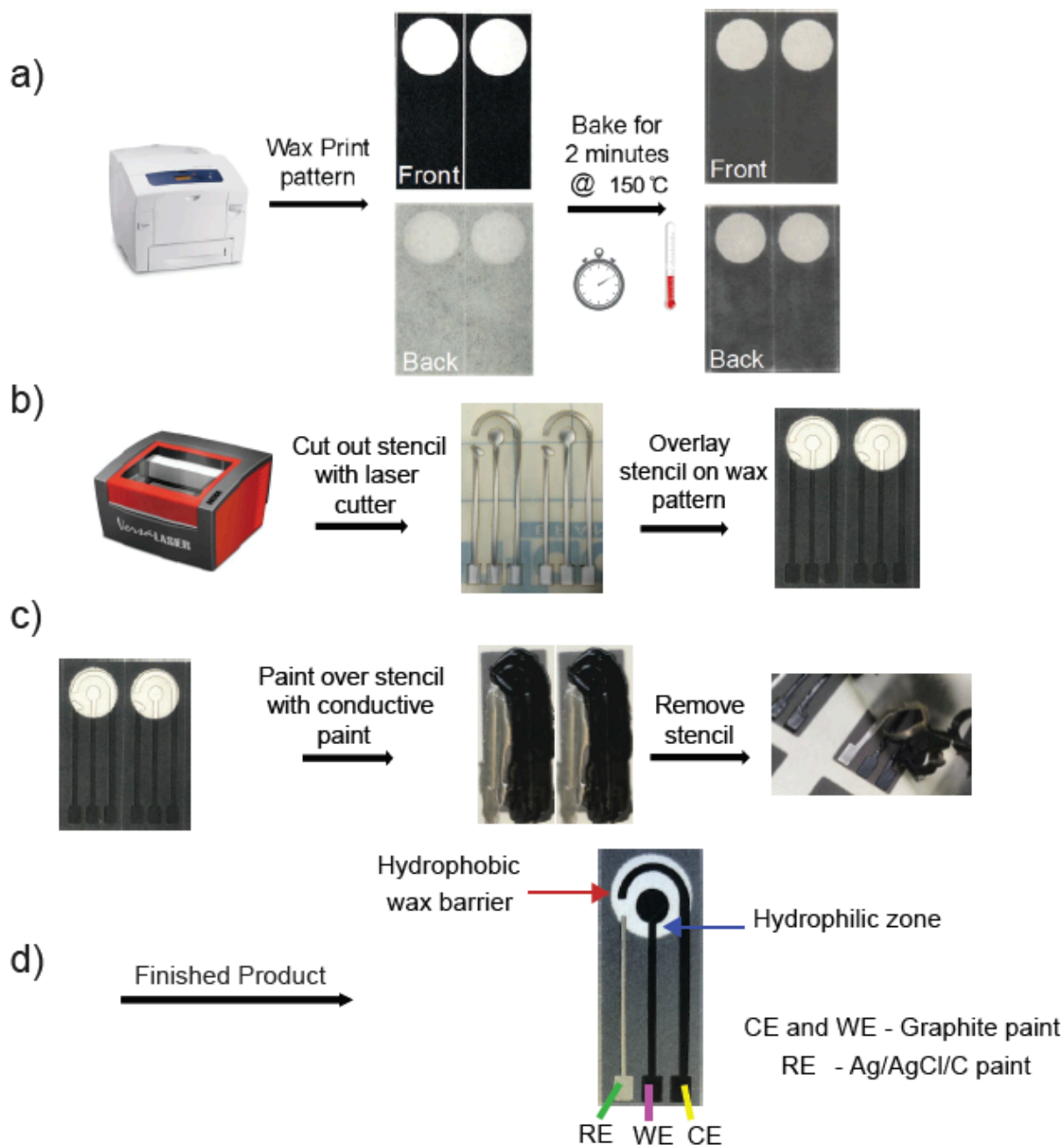


Figure 5. Fabrication of electrochemical paper-based device. a) A pattern is printed on filter paper to form the hydrophobic and hydrophilic zone. b) A plastic stencil is cut out following the design using a CO<sub>2</sub> laser cutter, the stencil is then placed over the wax-patterned devices. c) The electrodes are painted with conductive inks. d) The stencil is removed and the devices are allowed to dry, the sheet is then cut into individual devices.

### 4.3 Proof of Concept

#### 4.3.1 Unpolished vs. Polished Paper-based Devices

As a preliminary experiment, we adapted Compton's work on GCE and EPPG electrodes and tried to polish the electrodes of our PBD as the polished surface was critical for GCE and EPPG electrodes. Polishing the graphite-painted electrode would allow the formation of oxo-groups such as quinone on the surface and thus, the study of the effect of pH. To the best of our knowledge, this is the first report of polishing electrodes painted on PBD. The device was polished using a polishing pad typically used for semi-micro electrodes (figure 6a). In figure 6b a photograph of the paper-based device before and after it was polished is shown.

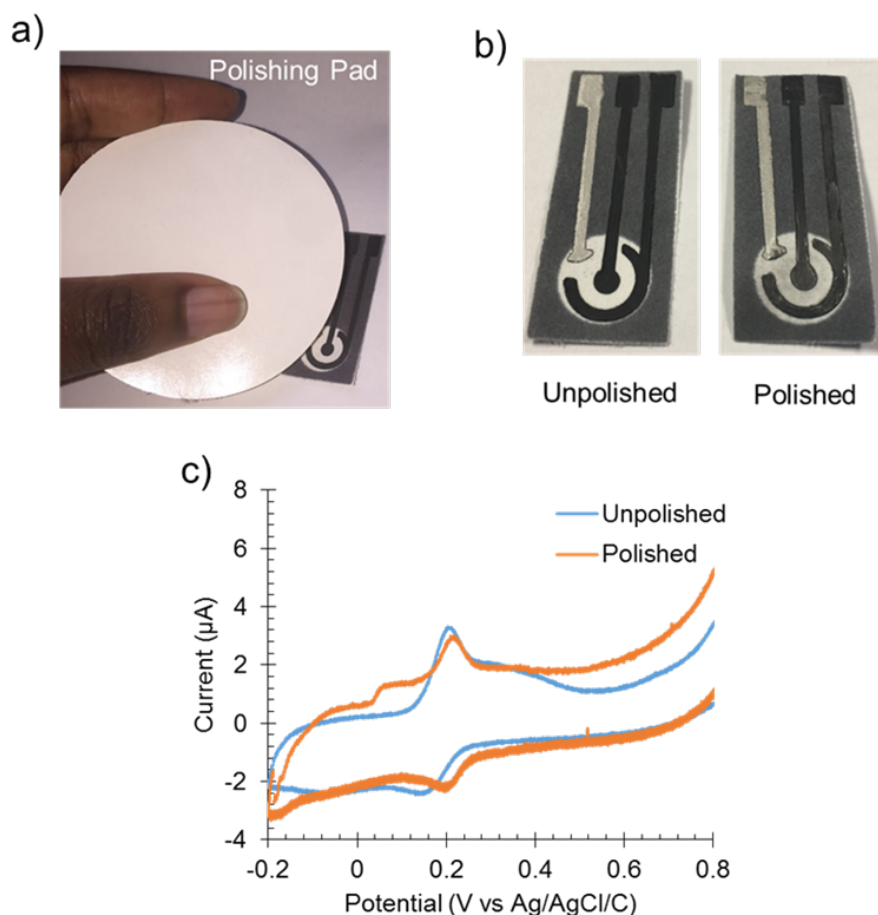
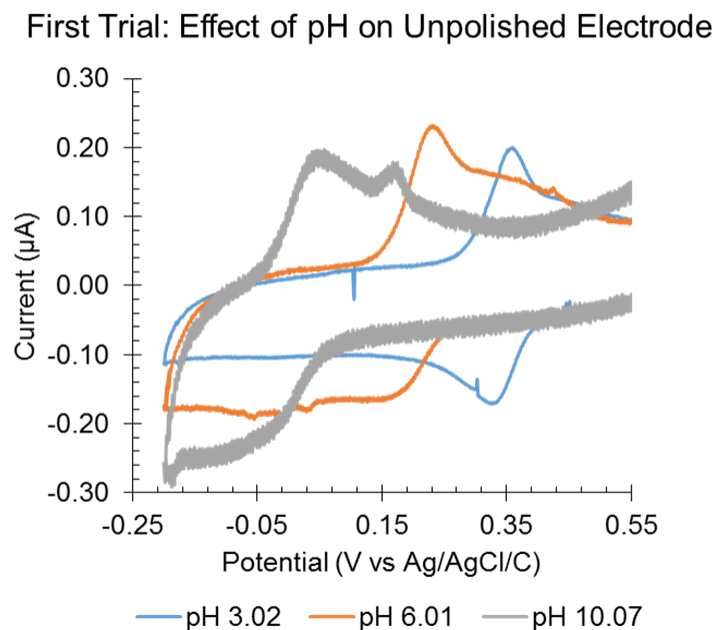


Figure 6. a) Photograph of a polishing pad. b) Paper-based device before and after polishing. c) Overlay of CVs for the unpolished device (blue) and the polished device (orange) tested in a 0.1 M HCl/0.1 M KCl solution at pH 3.0

To assess the effect polishing had on the electrodes, we compared CVs acquired with the unpolished device, and CVs acquired after polishing. Figure 6c is an overlay of these CVs in a solution of 0.1 M HCl/0.1 M KCl at pH 3.0. From the CV for the polished device (orange) in figure 6c, the ability to act as an electrode and generate redox peaks is unaffected, which meant the action of polishing did not damage or break the device. Unexpectedly, however, the redox peaks supposed to be from an oxo-group, on the unpolished device was already well defined. Since polishing displayed similar electrochemical results as not polishing, we decided to study the effect of pH on unpolished devices, thus eliminating a fabrication step. To determine if the redox reactions observed on an unpolished device was indeed pH dependent and could permit pH sensing, three solutions of pH 3.0, 6.0, 10.0 were tested on the device. The CVs of the three different solutions (figure 7) show a shift of the redox potentials of the peaks as pH increases which indicates presence of electroactive elements sensitive to pH.



*Figure 7. Cyclic voltammograms showing the shift of redox potential as pH increases. The scan rate was 50mV/s and the solutions prepared with HCl and NaOH.*

### 4.3.2 Unpolished PBD: Testing Different Buffers

As the first preliminary test was successful, we expanded the range of the pH tested. Two buffers were selected, Mcllvaine buffer and phosphate buffer. We chose Mcllvaine buffer because it is often reported for the development of pH sensors.<sup>28, 30</sup> It has a pH ranging from 3 to 8 which allows for probing around neutral pH. We also tested phosphate buffers, as they are commonly used in biological samples. They have a pH range from 5 to 9. Figure 8a is the overlay of the CVs obtained when testing various Mcllvaine buffer solutions at different pH. The CVs displays a shift in redox peaks potential as pH increases, as confirmed by the calibration curve in figure 8b (average over two CV cycles for each pH). A linear correlation is obtained when fitting the data with an  $R^2$  value of 0.9696, which confirms the presence of usable electroactive pH sensing elements on the electrode. Figure 9a is an overlay of CVs taken after testing solutions made with 0.1 M phosphate buffer at different pH. A shift in potential of the redox peaks as pH increases is also observed. The calibration curve in figure 9b has a linear response with an  $R^2$  of 0.9941. The results acquired from the two buffers confirm that there are groups on the surface of the electrodes on the PBD device that are pH dependent and indicate the opportunity to develop a paper-based electrochemical pH sensor.

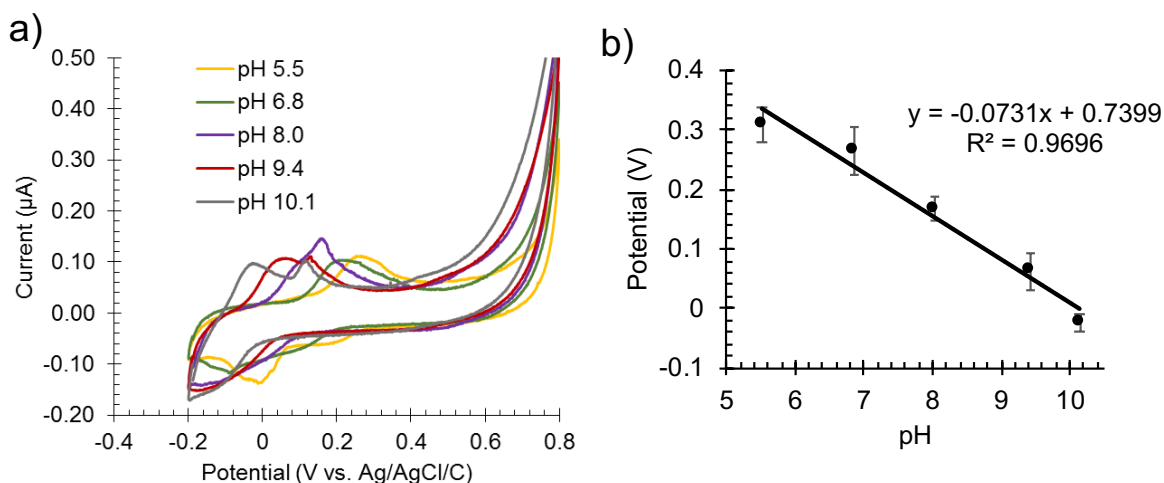


Figure 8. a) CV overlay of Mcllvaine buffers (pH 3 to 8) and NaOH/HCl solutions (pH 9 and 10). b) Calibration curve for the potentials of cathodic peaks done over the average of two cycles for each sample.

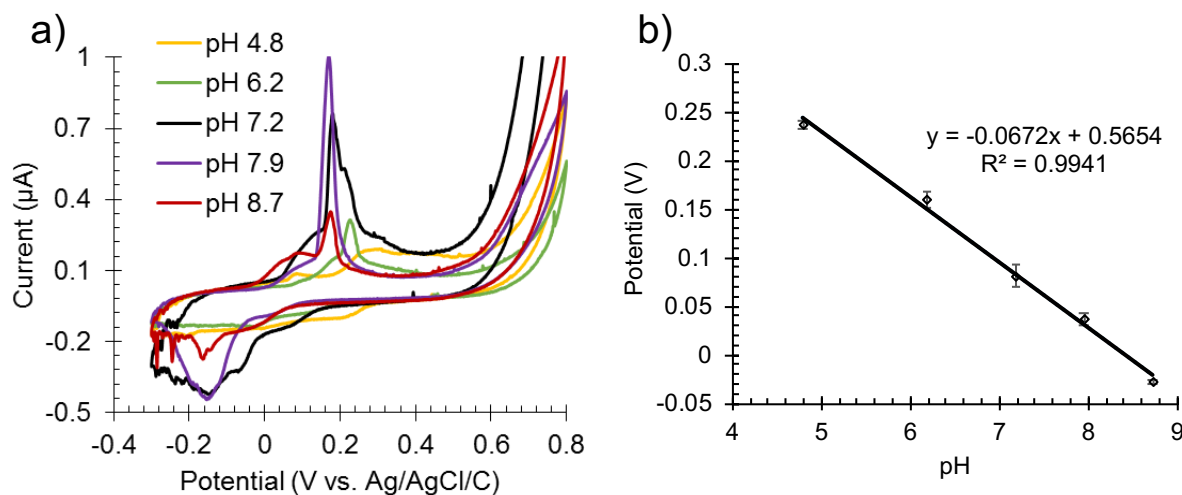


Figure 9. a) CV overlay of phosphate buffer pH 5 to 9. b) Calibration curve for the potentials of cathodic peaks done over the average of two cycles for each pH.

#### 4.3.3 Data Analysis: Software vs. Manual Peak Picking

A critical step in interpreting electrochemical data such as CVs involves determining the potential of the peak and its associated maximum current. Most instruments allow for estimation of these values on their dedicated software while acquiring the data. For accurate determination of the values, the data are typically processed separately after acquisition. The preliminary data analysis was done by using excel to approximate the correct values for each peak potential. We then used an open source software called eL-Chem Viewer developed by Hrbac *et al.*<sup>52</sup> We established an illustrated step-by-step procedure to use eL-Chem Viewer. The reduction potential of the peaks were collected manually and then again with the software, and calibration curves were generated (Figure 10). The calibration curve for manual data (Figure 10a) has an  $R^2$  value of 0.9301 and the curve for data collected using software (Figure 10b) has an  $R^2$  value of 0.9696. For both curves the potential decrease as pH increases, however the fitting using values determined with the software shows a better linear correlation than peaks manually picked up.

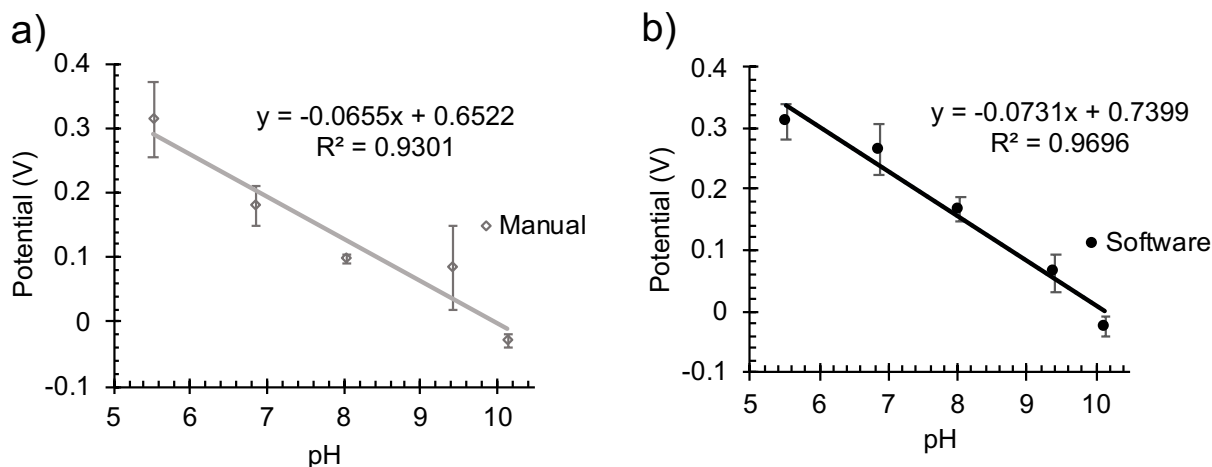


Figure 10. a) Calibration plot of peak values collected manually from excel b) calibration plot of values collected using the software eL-Chem viewer.

#### 4.3.4 Assessment and Problems Encountered

Due to the lack of control on the formation of the pH-dependent group on the electrode, the potential variability in manual fabrication of the PBD, and small currents involved, the repeatability of the method using paper-based device to measure pH needed to be assessed. A series of tests were conducted on three paper-based devices, a total of five trials were run on the three devices. Each trial counted two cycles or CVs. The potential of reduction peaks of CVs for each pH were collected using the software and the data was plotted; the overlay of these plots is displayed in figure 11. A good correlation is observed between all trials (Figure 11a). We noticed with preliminary tests that results for solution with a pH lower than 5 were inaccurate as they did not follow the same trend. After removing the data for pH below 5 (Figure 11b) the  $R^2$  values of all calibration curves improved greatly: out of 10 trials 6 now displayed a  $R^2$  of 0.985 or above. Figure 11c shows the average and standard deviation of all data. These data highlights that in those conditions the devices have a standard deviation larger than desired.



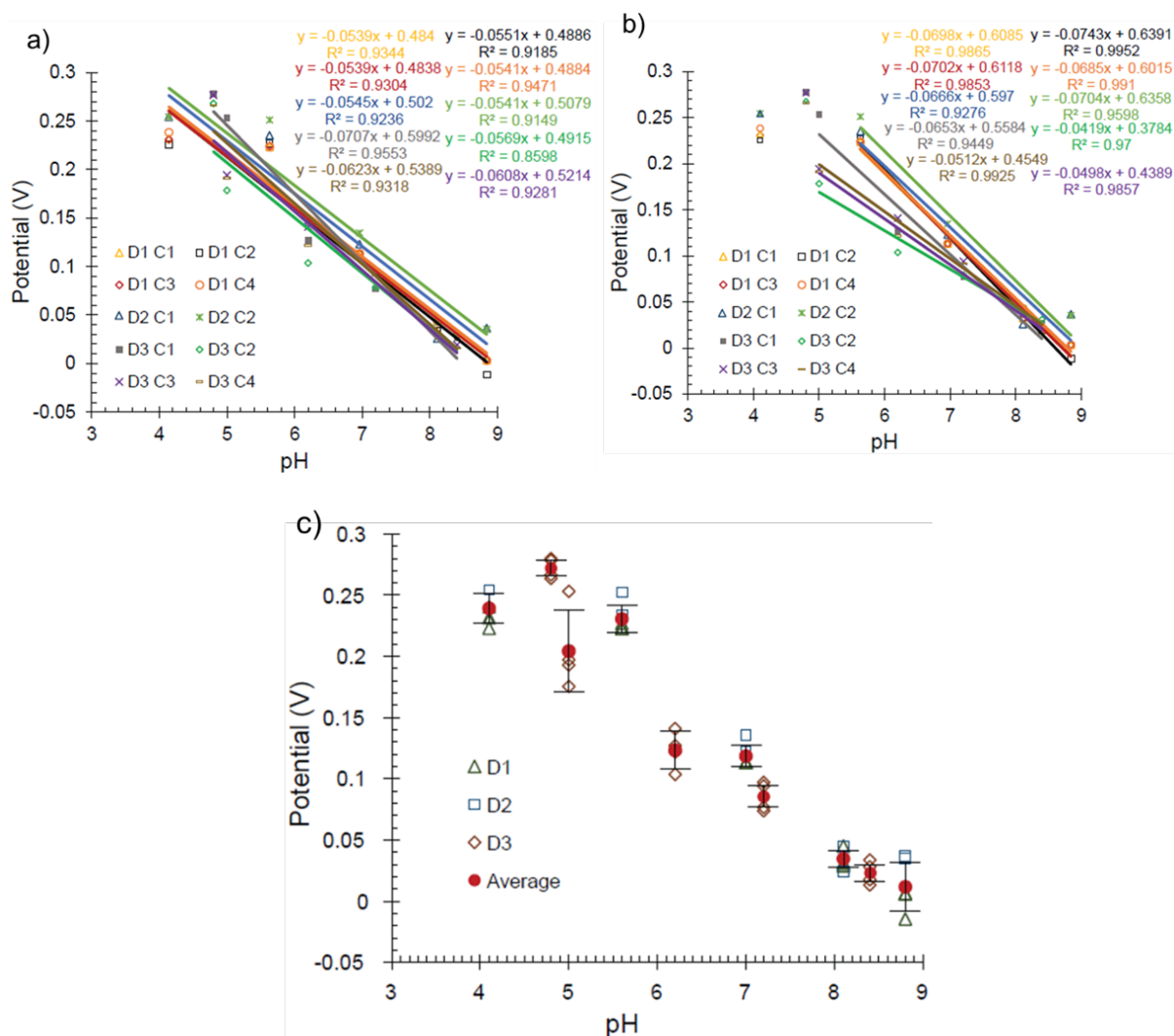


Figure 11. Assessment of method to measure pH on PBDs, CVs on D1, D2, D3 using phosphate buffers with pH values ranging from 5 to 9. a) Overlay of calibration curves of three devices over five trials with two cycles each. b) Overlay of calibration curves without data points from solutions with pH below 5 included in the linear fit. c) Potentials of reduction peaks of all CVs plotted with the average and standard deviation.

Preliminary testing done on the paper-based devices yielded promising results. Some issues were however encountered as we conducted more experiments. These results showed that repeating the method with different PBDs, we can obtain similar trends. The future goal of this project is to apply the developed pH sensor to oral preventative care where pH 3 to 6 will be critical, we needed to address the difficulties of measuring pH below pH 5. Along with the difficulties measuring low pH, we had problems with CVs on the PBDs: many paper-based devices would have CVs with well-defined redox peaks and relatively large current (as seen in figure 8), however,

some would barely have peaks, while others had no peaks. Examples of peaks not well defined are shown in figure 12. Figure 12a is the CV of a solution of McIlvaine buffer at pH 3, it only shows some noisy (multiple peaks) oxidation peaks which are not the peaks that correspond to the redox reaction of quinone at pH 3. Figure 12b is the CV of a solution of phosphate buffer at pH 5, the redox reaction is not visible on the CV. Optimization of the method was thus necessary to achieve observable redox peaks on most devices at all pH values.

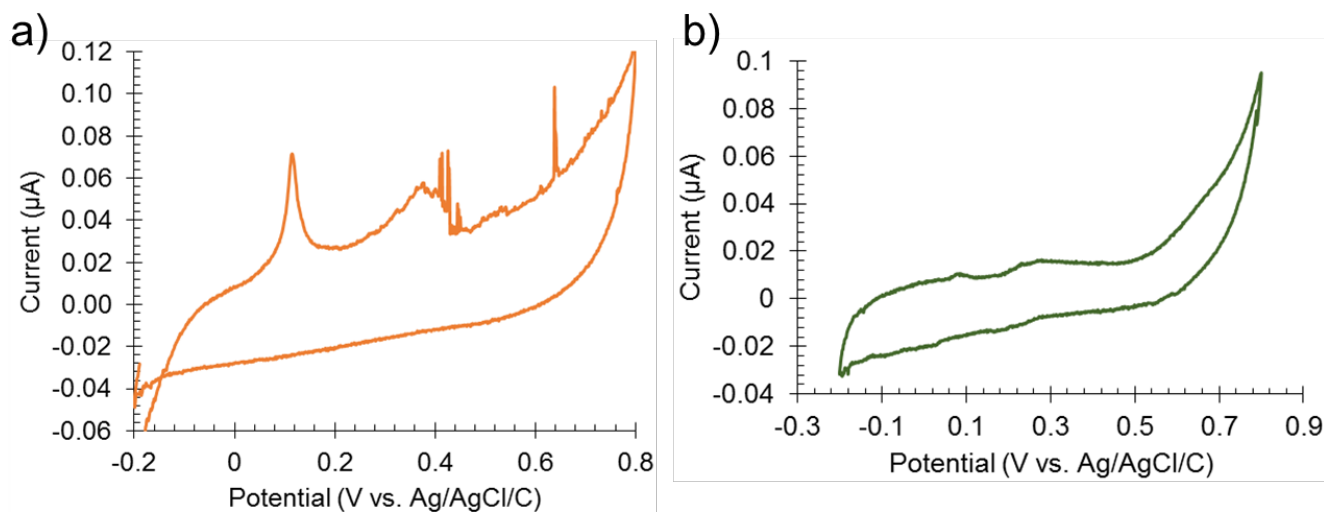


Figure 12. a) CV of McIlvaine buffer at pH 3, noisy peaks b) CV of phosphate buffer at pH 5, peaks not visible.

#### 4.4 Conclusion

A low-cost, flexible and portable electrochemical paper-based device to be used as a pH sensor was successfully developed. Preliminary tests showed that pH can be determined on polished and unpolished paper-based device, and thus for the rest of the project unpolished devices were used. A shift of the potentials of the redox peaks as pH increases was observed with the different buffers (McIlvaine and phosphate) tested, thus indicating the presence of electroactive elements sensitive to pH on the surface of our electrodes. Data analysis was improved and facilitated by using the software eL-Chem Viewer and developing a step-by-step procedure. Multiple devices were used to assess the method developed. The different trials and cycles repeatedly produced a linear response despite a low precision. The next chapter will focus

on optimization methods to improve the definition of the peaks observed on the paper-based devices.

## CHAPTER 5. MODIFICATION OF PAPER-BASED DEVICES TO IMPROVE REDOX PEAKS

This chapter focuses on different treatments of the electrodes to increase the presence of pH-dependent electroactive oxo-groups on the surface of the electrodes. These treatments were intended to overcome issues with the paper-based device (absence of defined peaks, no results at low pH). Several approaches have been used to increase functional groups or improve the redox reaction at the surface of carbon materials. Some of these approaches include the adsorption of pH sensitive polymer films on the surface of the electrode,<sup>13, 28</sup> chemical modification, and attachment of quinone derivatives on the surface of the electrode.<sup>48, 53-56</sup>

### 5.1 Sodium Carbonate Treated Paper-based Devices

The modification of carbon material involving the immobilization or induced formation of functional groups that contain oxygenated species has been well studied.<sup>27</sup> The immobilization of oxygenated species on graphite was reported by Craig E. Banks and coworkers.<sup>27</sup> In this study they chemically pretreated a graphite screen-printed electrode by immersing the electrode into a percarbonate solution overnight to form oxygenated species on the electrode surface to accurately measure pH.

We adapted this method by performing a modification on our paper-based devices to determine if such treatment could improve the redox reaction observed. We dipped the paper-based electrodes into 1 M sodium carbonate overnight before using them in pH experiments. Figure 13a shows the CV overlay of the chemically pretreated paper-based device using the procedure described in detail in the Chapter 3: Experimental section. The CVs were run using solutions of 0.1 M phosphate buffer at various pH values ranging from pH 5 to 9. In figure 13a we observe redox peaks that are very noisy which could be due to the immobilization of excess sodium carbonate on the surface of the electrode. No distinct differences between treated and untreated paper-based devices were observed, as neither the definition of the redox peaks nor the current improved. The calibration curve in figure 13b of the anodic peaks shows a linear response with an  $R^2$  of 0.9647, whereas the calibration curve for the cathodic peaks (Figure 13c) showed an even

poorer linear response. Both results are comparable to the data obtained without treatment of the paper-based devices.

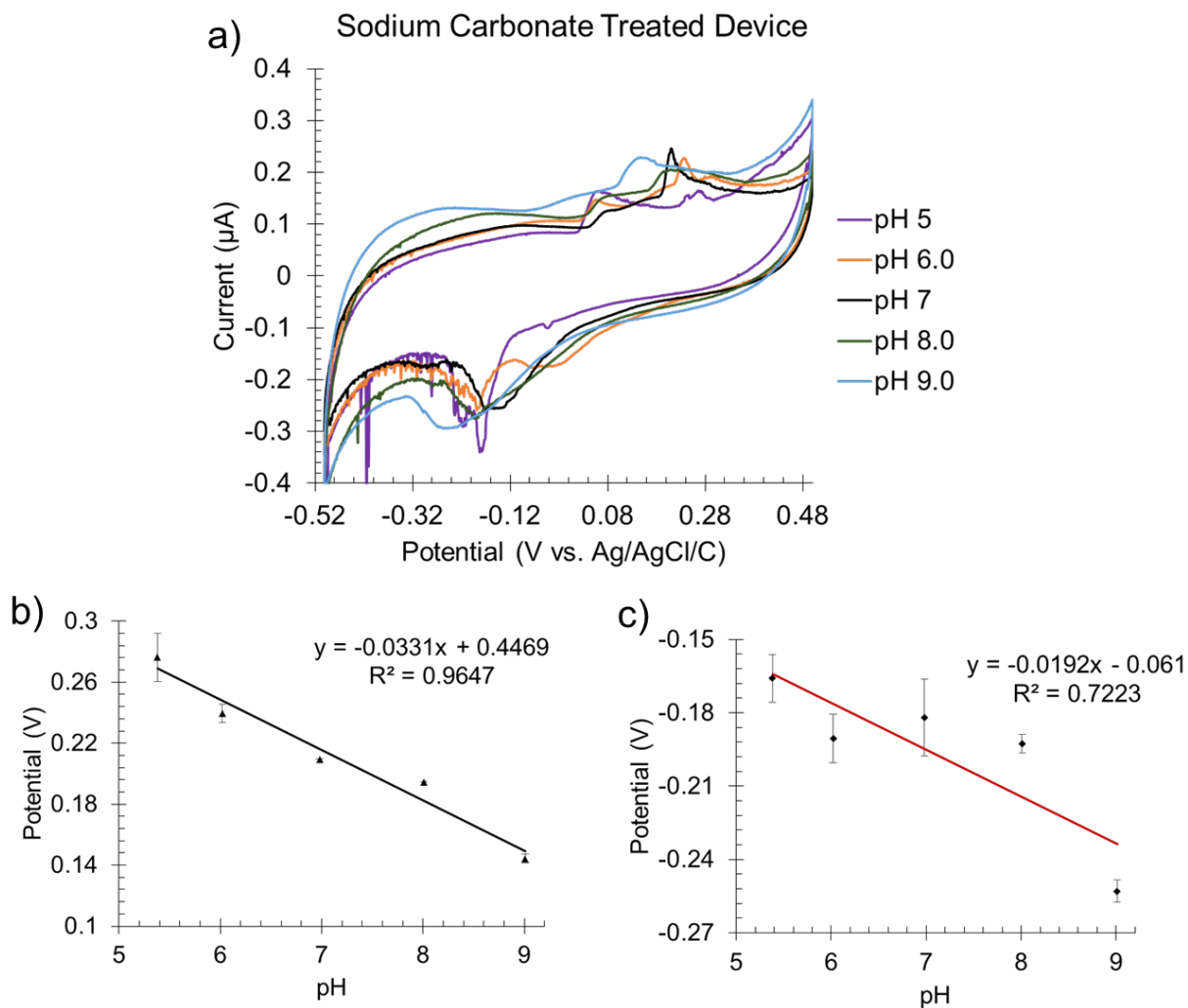


Figure 13. a) Overlay of CVs collected using sodium-carbonate-modified PBD, solutions of 0.1 M phosphate buffer with pH values ranging from 5 to 9. b) Calibration curve of the oxidation potential peaks. c) Calibration curve of the reduction potential peaks.

## 5.2 Square Wave Voltammetry (SWV)

The peaks observed on the CVs after sodium carbonate were particularly noisy with small current. We hypothesized that a different electrochemical technique could help: Square Wave Voltammetry (SWV). In SWV, the cell current is measured as a function of time and as a function of the potential between the indicator/working and reference electrodes, a square-wave potential wave form is applied over the linear scan of potentials. The purpose for using this technique was

to take advantage of a typical effect in SWV of suppressing background noise to obtain better defined redox peaks. Figure 14a shows the SWV of a carbonate pretreated paper-based device tested with various pH solutions of 0.1 M phosphate buffer ranging from pH 5 to 9. The reduction peaks in this figure shift from 122 mV to -58 mV as the pH increases. The calibration curve for the SWV (Figure 14b) has a linear response with an  $R^2$  of 0.9934. The  $R^2$  values for the redox reaction for the CVs was 0.9647 for the oxidation and 0.7223 for the reduction peaks compared to the  $R^2$  value of 0.9934 for the SWV. Comparing data from the CVs and the SWV for the carbonate pretreated device there is a clear improvement with the linear response. After repeating the experiments for a few trials, however, such an improvement appeared to be random. Some carbonate pretreated devices gave good results when using the SWV, but there were a few devices that presented no peaks shifting with pH neither with CVs nor SWV.

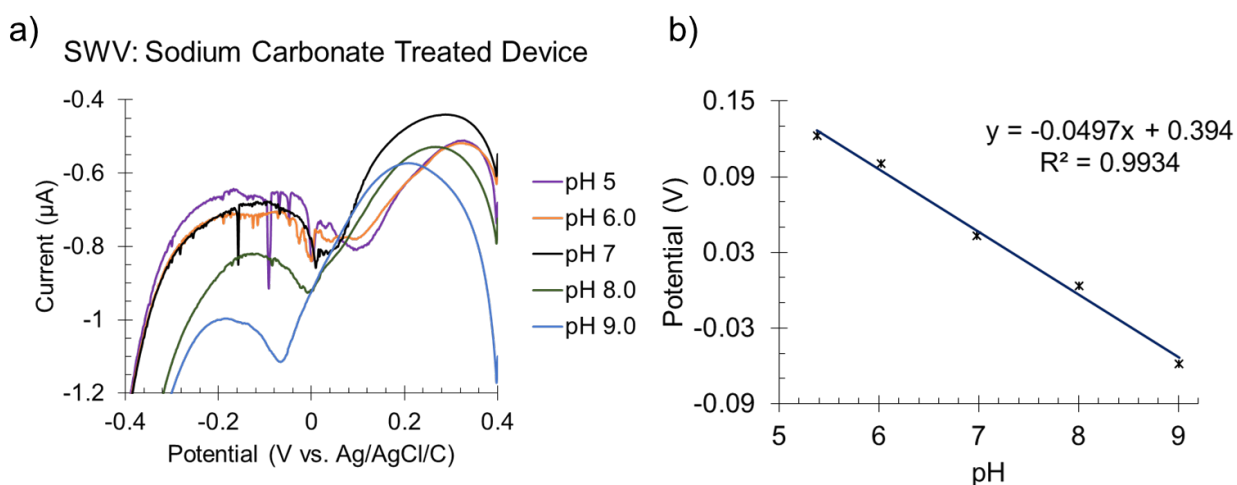


Figure 14. a) Square Wave Voltammograms of sodium carbonate pretreated device. b) Calibration curve of SWV peaks.

We decided to try a different method to improve the presence of the oxygenated species on the electrode surface of our paper-based because the results from sodium carbonate pretreatment were irreproducible. We continued to run both CV and SWV, but as SWV did not present clear improvements and CV give more information on the decorrelated oxidation and reduction waves, we focused more on CVs for the rest of this thesis.

### 5.3 Plasma Treatment

#### 5.3.1 Oxygen Plasma Treatment using Air

Another approach for the improvement of the definition of the redox peaks was to activate or enhance the formation of the oxygenated species at the surface of the electrodes by oxygen plasma. We used a plasma cleaner to treat our devices with an oxygen (air) plasma. Many reports mention using oxygen plasma treatment for sensing devices mainly for the fabrication of polydimethylsiloxane (PDMS)<sup>57,58</sup> microfluidics devices where the surface properties are changed from being hydrophobic to hydrophilic to facilitate modification and bonding of surfaces. Evans and Kuwana<sup>59</sup> studied the use of oxygen plasma treatment on pyrolytic graphite electrode surface for the formation of the surface oxygen-containing functionalities which mostly include carboxyl and hydroquinone/quinone groups.

The oxygen plasma treatment is done by introducing oxygen (from the ambient air) into the chamber of a plasma cleaner under high intensity radiofrequency (RF). The formation of plasma is observed via a purple-pink color in the chamber. The device is exposed to the plasma for 3 minutes. Figure 15a shows the CVs of an oxygen plasma treated device using different solutions of 0.1 M phosphate buffer with pH values ranging from 5 to 9. Calibration plots of anodic and cathodic peaks potential (Figure 15b and 15c, respectively) show an improvement in the linear responses.

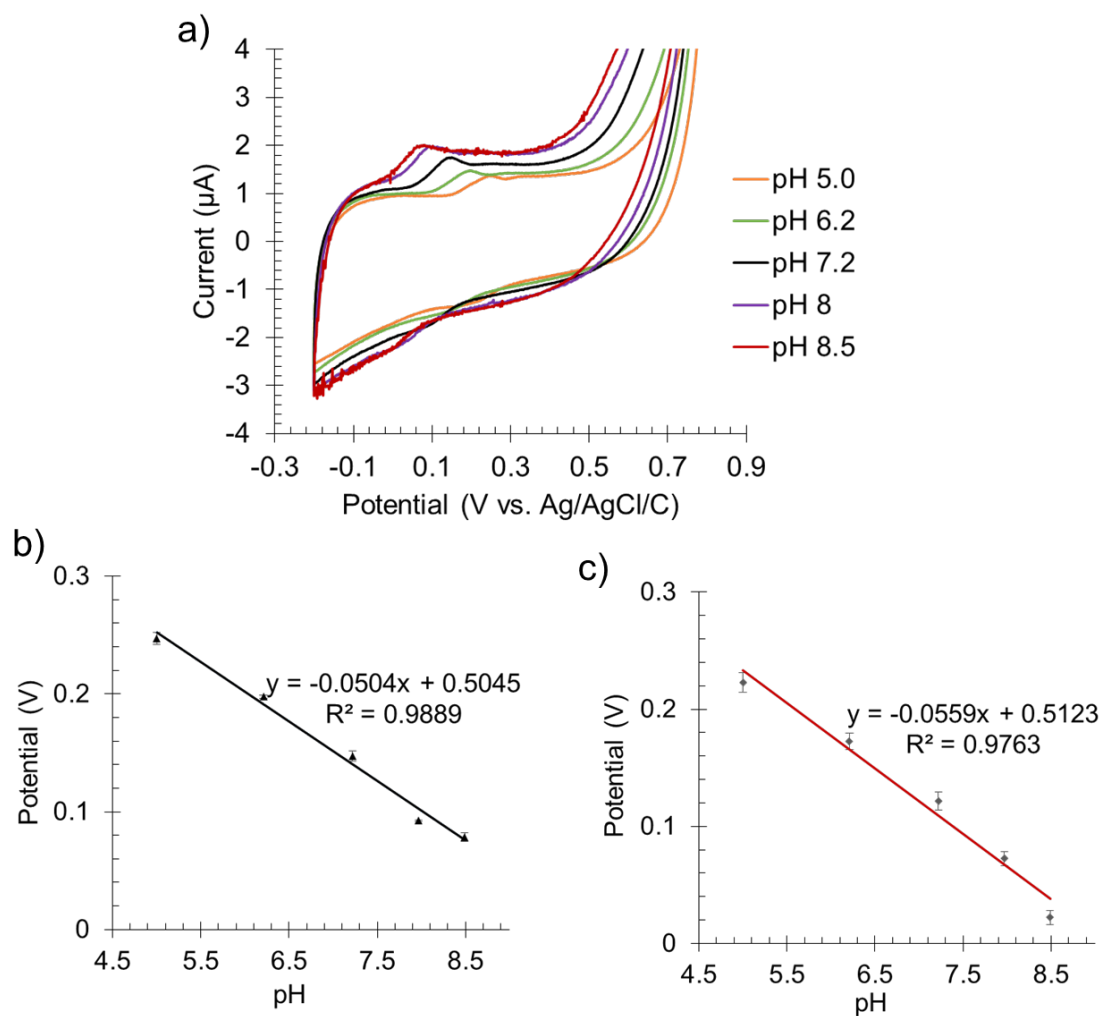


Figure 15. a) CVs of an oxygen plasma treated paper-based device in 0.1 M phosphate buffer with pH values ranging from 5 to 9. b) Calibration curve of the oxidation peaks. c) Calibration curve of the reduction peaks.



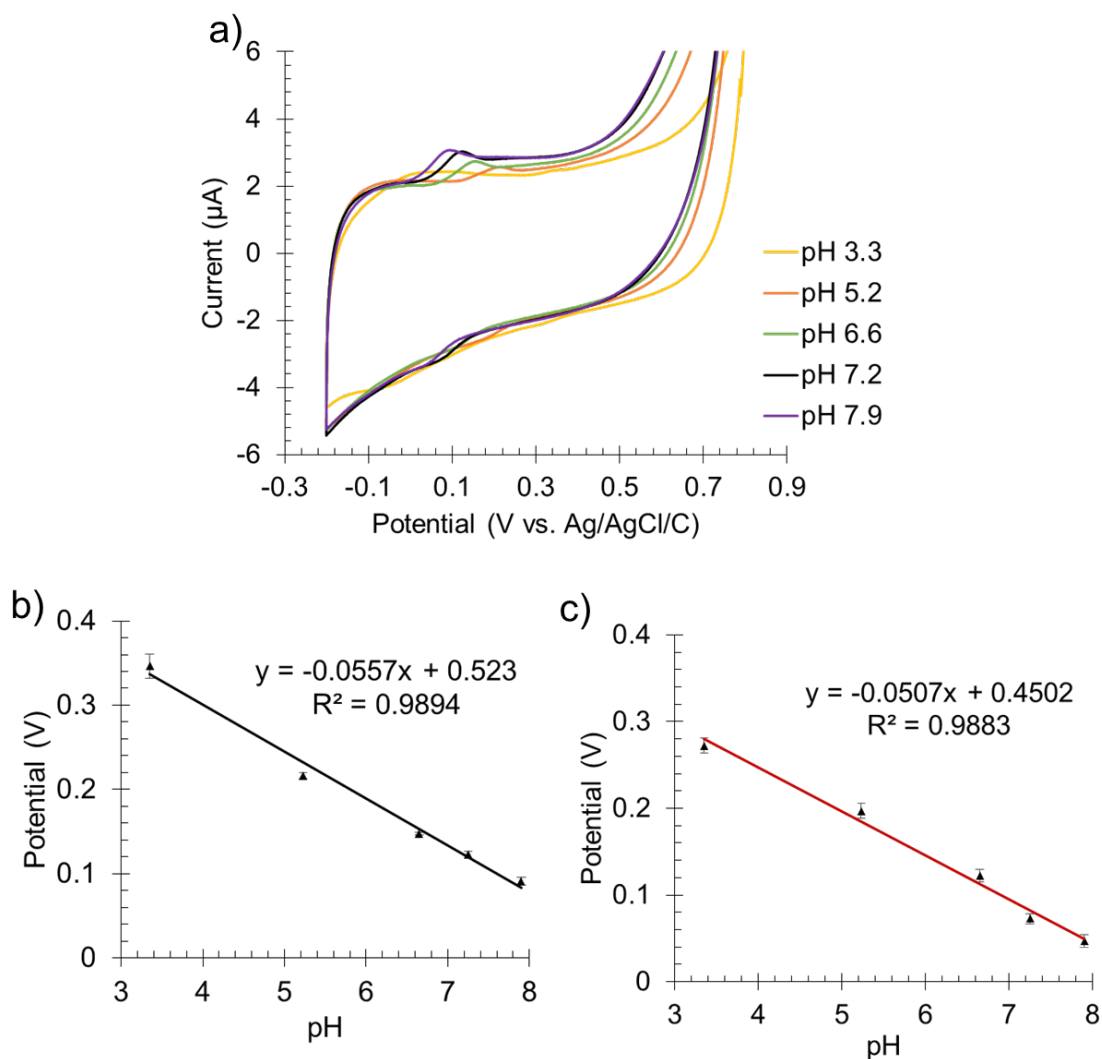


Figure 16. a) CVs of an oxygen plasma treated paper-based device in McIlvaine buffer with pH values ranging from 3 to 8. b) Calibration curve of the oxidation peaks. c) Calibration curve of the reduction peaks.

Following the same method new paper-based devices were plasma-treated and tested using various solutions of McIlvaine buffer with pH values ranging from 3 to 8 (Figure 16a). Figure 16b and figure 16c are calibration curve for the potential of the anodic peaks and all the potential of the cathodic peaks respectively. The plasma-treatment results show no noise and well-defined peaks, thus leading also to a better correlation between peak potentials and pH for the plasma-treated paper-based devices compared to untreated devices.

We tested the repeatability of the new method by performing the plasma treatment on multiple devices. The results from these tests were not always repeatable (Figure 17). The tests were done using samples of phosphate and Mcllvaine buffer at different pH.

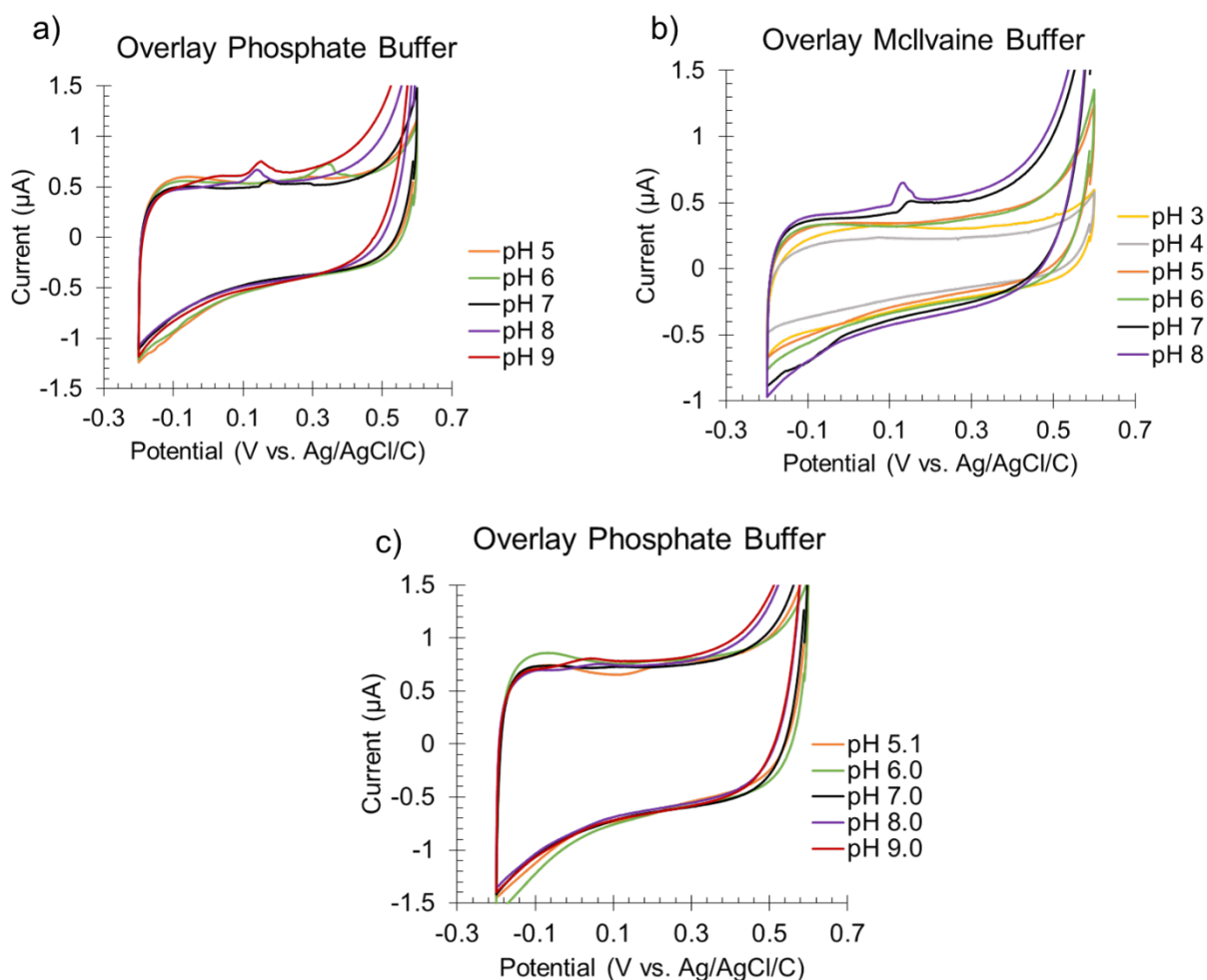


Figure 17.a-b) Overlay of CVs of phosphate and Mcllvaine buffers using the same plasma-treated device. c) Overlay of CVs of phosphate buffer on another plasma-treated device.

Figure 17a is the CV overlay for pH solutions of phosphate buffer, and only shows small anodic peaks on the CVs of solution at pH 8 and 9. On the figure 17b which is the CV overlay for solutions of Mcllvaine buffer using the same PBD as figure 17a, we observe small anodic peaks on the CVs of the solutions at pH 8 and 9. Figure 17c is the CV overlay for pH solutions of phosphate buffer on a different plasma-treated device, there are small anodic peaks visible for all solutions. None

of the CVs in the figure 17 display reduction peaks, thus indicating that the method needed more optimization.

### 5.3.2 Oxygen Plasma Treatment using Pure Oxygen

As seen above with the plasma treatment using ambient air containing oxygen, there were more devices with no redox peaks than devices with redox peaks. We hypothesized that using pure oxygen instead of “air” plasma might yield better and repeatable results. The oxygen pressure was set at 10 psi and introduced into the chamber with an optimized flow rate of 22.5 ml/min. The devices were exposed to the plasma (high RF) for 3 minutes. The device with the sharpest redox peaks for a sample of 0.1 M phosphate buffer at pH 7 was selected for further experiments (Figure 18a) with different solutions of phosphate buffer with pH values ranging from 5 to 9. Figure 18b is a CV overlay of the oxygen plasma-treated device at the different pH. The well-defined peaks display a clear shift to more negative potentials as the pH increases. The calibration curve for the anodic peaks (figure 18c) shows a linear response with an  $R^2$  value of 0.9716, and the calibration curve for the cathodic peaks (figure 18d) shows a linear response with an  $R^2$  value of 0.9719, the  $R^2$  values did thus not improve. Using the same PBD a SWV experiment was performed with the following parameters: frequency 3 Hz, amplitude 200 mV with different solutions of phosphate buffer with pH values ranging from 5 to 9.

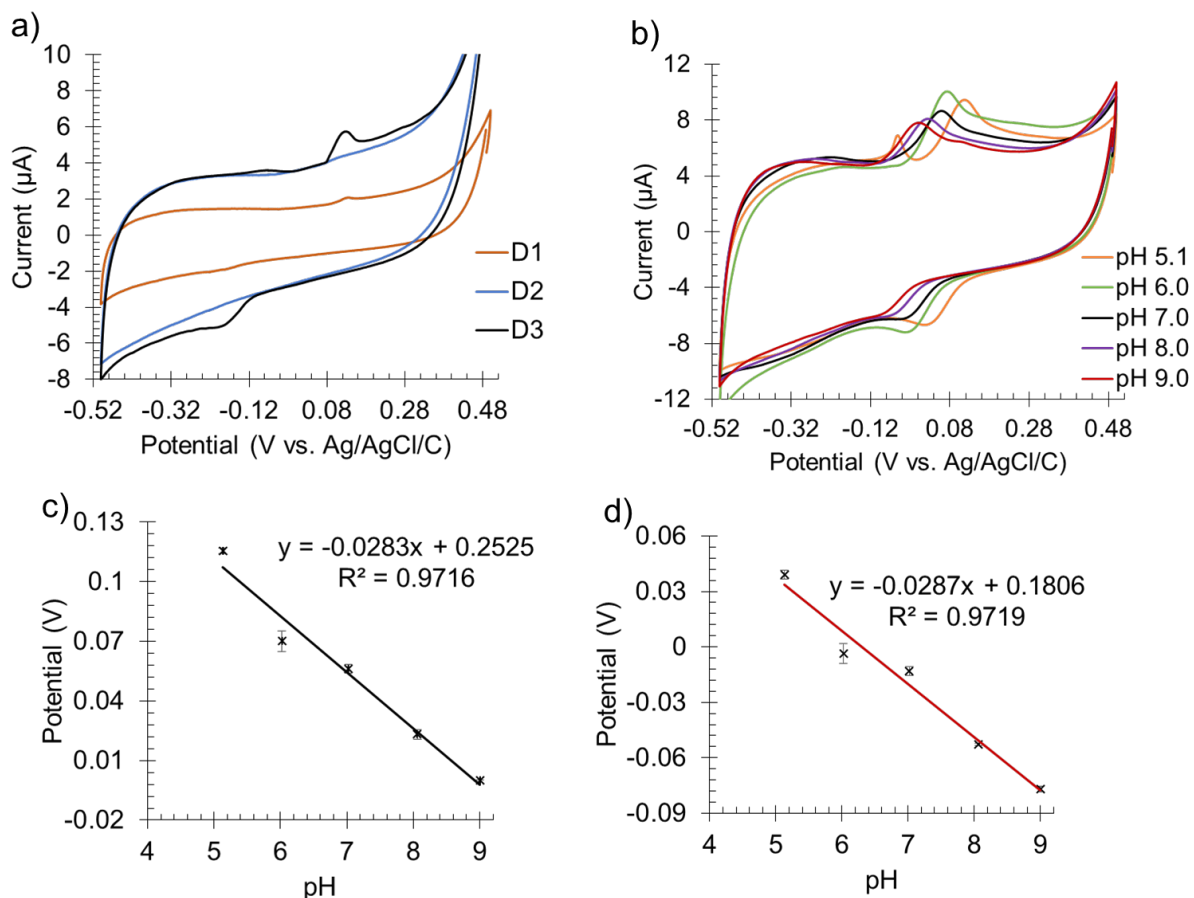


Figure 18. a) Overlay of CVs of different devices used to screen for the device with well-defined redox peaks. b) CV overlay of pure oxygen plasma treated device. c) Calibration curve of oxidation peaks. d) Calibration curve of reduction peaks

The SWV overlay (Figure 19a) shows the redox peaks shifting as pH increases, the calibration curve (Figure 19b) shows a good linear correlation with an  $R^2$  of 0.9875. Results from the SWV are complementary to the results from the CVs with a small improvement. When comparing the CVs collected before the oxygen plasma treatment was done to those collected after the plasma treatment, we observe a great increase in the capacitive current. The oxygen plasma treatment on the paper-based devices caused a modification on the device that leads to an increase of the capacitive current of approximately 10 folds (Figure 20). The electrochemical oxidation of carbon material enhanced the effect of the electrode capacitance,<sup>60</sup> thus increasing the intensity of the capacitive current.

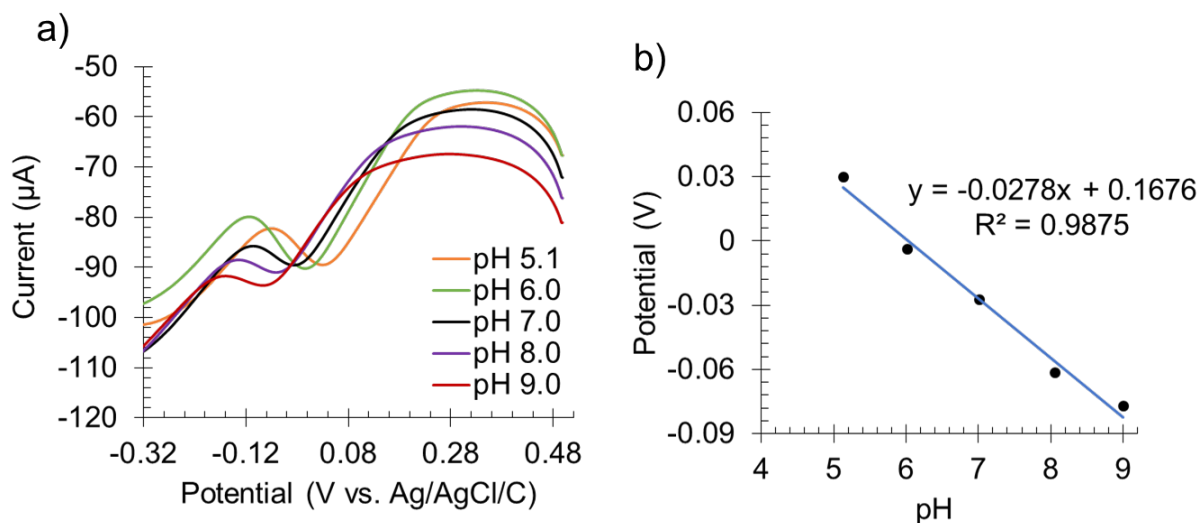


Figure 19. a) Overlay of SWV collected in different phosphate buffers with pH values ranging from 5 to 9. b) Calibration curve of potential peaks.

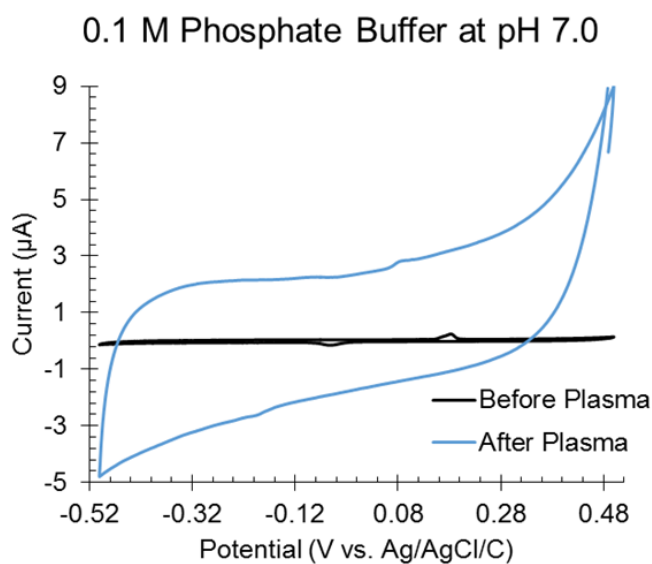


Figure 20. CVs collected before and after plasma treatment to demonstrate the increase in capacitive current

### 5.3.3 Effect of Plasma on Reference Electrode

When analyzing CVs before and after the oxygen plasma treatment, we noticed that there was a shift or translation in the potential of all the redox reactions. Additionally after plasma treatment, the color of the reference electrode changed from silver to black (Figure 21a-c). To

determine the cause of the shift in potential of redox reaction on the CVs, we conducted an experiment where the reference electrode was removed from the plasma treated device and replaced with a reference electrode from an untreated device. All trials were tested using a sample of 0.1 M phosphate buffer at pH 7.0. The first CV was run on an untreated device (figure 21a), the device was dried for over 30 minutes and placed in the plasma cleaner for oxygen plasma treatment with the parameters listed above, and the second CV was run using the same solution. The blackened reference electrode was cut out (figure 21b) and replaced with a new reference electrode from an unused device (figure 21c). Finally a CV was run using the same solution and the three CVs were overlaid (figure 21d) to compare the location of the different redox peaks potential. The potential of reduction peaks was - 75 mV for before plasma, - 193 mV after plasma and - 81 mV after the RE is cut and replaced. The change in the color of the reference electrode suggests that the Ag/AgCl/C paint has oxidized during the plasma treatment. The redox shift caused by the oxidized reference electrode explains the effect of the linear response being translated to more negative when comparing results of untreated electrodes with results of oxygen-plasma treated devices.

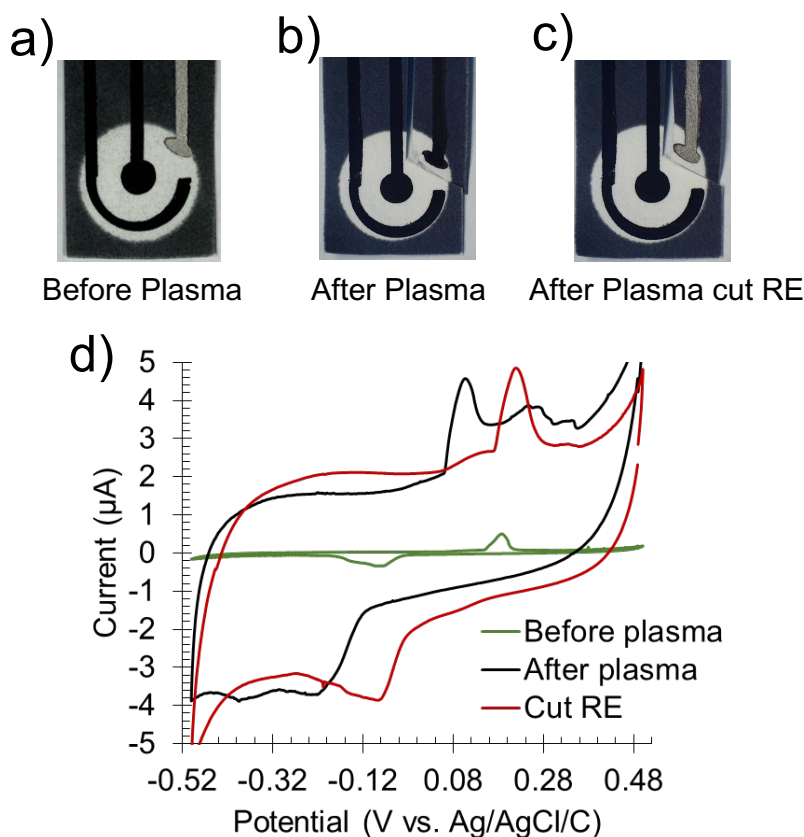


Figure 21. a) Paper-based devices before plasma, b) after plasma, and c) after the reference electrode is cut and replaced. d) CVs of Oxygen plasma treated device

#### 5.4 Conclusion

Various approaches for the enhancement of the definition of redox peaks on the CVs were described in this chapter. The results of the chemical modification of the electrode with oxygenated species using sodium carbonate showed a lack of repeatable improvement compared to unmodified devices. The treatment of the surface of the electrode to expose more defect site to react with oxygen forming the functional groups was done in two ways: oxygen (ambient air) plasma treatment and pure oxygen plasma treatment. The offset in redox peaks after treatment was due to the oxidation of the reference electrode during the oxygen plasma-treatment. None of the methods yielded repeatable and noticeable improvements, thus additional optimization was necessary to improve the presence and definition of pH-dependent redox peaks.

## CHAPTER 6. CHANGES TO THE DESIGN OF DEVICE AND CONDITIONING STEP

### 6.1 Change in Design: Filter Paper

We evaluated different types of filter paper to fabricate the paper-based devices. The fabrication of the devices for all prior trials was done using Whatman® qualitative filter paper, Grade 114 with a pore size of 25  $\mu\text{m}$  and a flow rate of 100 mL/38 sec (manufacturer specifications). We assessed two additional filter papers. Grade P4 is a medium pore size of 5 to 8  $\mu\text{m}$  filter paper and a flow rate of 20 mL/60 sec (manufacturer specifications). Grade P2, with a pore size of 1 to 5  $\mu\text{m}$ , and a flow rate of 5 mL/60 sec (manufacturer specifications). We performed CV on the different paper-based devices with a sample of 0.1 M phosphate buffer at pH 7.0. An overlay of the CVs of the three devices was made (figure 22).

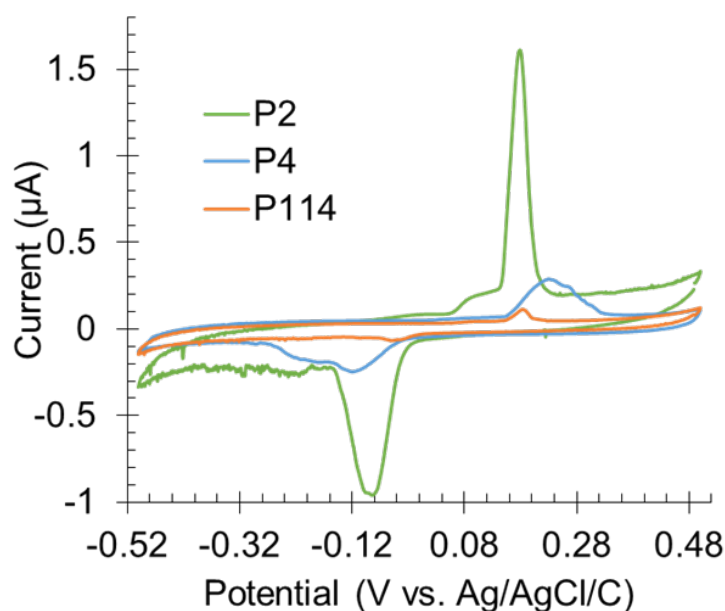


Figure 22. Comparison between different pore-size filter papers: filter paper P114, P4, and P2 have a pore size of 25 $\mu\text{m}$ , 5 to 8  $\mu\text{m}$ , and 1 to 5  $\mu\text{m}$ , respectively.

The CV for the P114 device has the smallest redox peaks, the CV for P4 device has broad and not well-defined redox peaks, and finally the CV for P2 device has the sharpest redox peaks.



Evaluation of more devices made with the three different filter papers in the same solution demonstrate that filter paper P2 continuously displayed the sharpest peaks.

The use of smaller-pore filter paper P4 and P2 showed that the peaks on the surface of the electrodes were better defined for both oxidation and reduction reaction. Statistics from the evaluation of 15 different paper-based devices for each of the three filter papers revealed that 66% of P114 devices, 80% of P4 devices and 86% of the P2 devices displayed well-defined redox reaction peaks. To confirm that using smaller-pore filter paper would consistently yield sharper peaks, we tested different solutions of 0.1 M phosphate buffer with pH range from 5 to 9 on P4 and P2 devices. The potentials of reduction peaks were collected from all the CVs for both filter paper and were plotted (Figure 23). The potentials of the peaks shift as the pH increases, following a linear response of the fitted data with an  $R^2$  of 0.9916 for P4 device and 0.9952 for P2 device. The results from figure 23 asserts that devices yield well-defined redox potential peaks that shift towards the negative potential as pH increases. The sharp peaks and 86% of the Grade 2 (P2) devices lead to the decision to continue all further experiments using P2 filter paper to fabricate the paper-based devices.

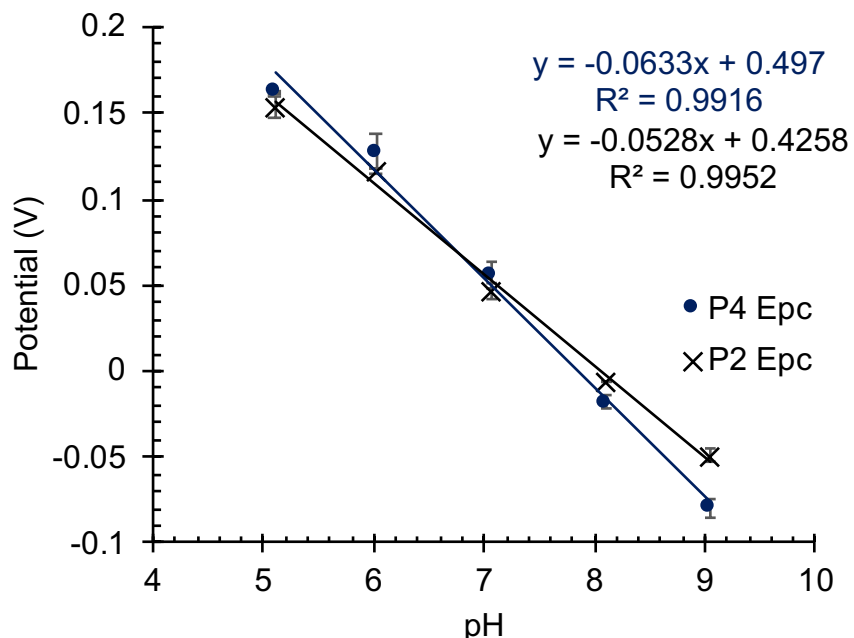


Figure 23. Calibration plot for smaller pore-size filter paper.

## 6.2 Change in Design: Area of Working Electrodes

In the three-electrode system for electrochemistry consisting of the working electrode (WE), the counter or auxiliary electrode (CE) and the reference electrode (RE); the working electrode is the electrode at which the reaction occurs. Changes made to the area of the working electrode directly affects the current as per the Randles–Sevcik equation (eq 3) assuming a diffusive system.

$$i_p = 0.446nFAC^0 \left( \frac{nFvD_0}{RT} \right)^{1/2} \quad (\text{eq. 3})$$

$i_p$  is the peak current (A),  $n$  is number of electrons transferred in the redox event,  $A$  is the electrode surface area ( $\text{cm}^2$ ),  $F$  is the Faraday Constant ( $\text{C}\cdot\text{mol}^{-1}$ ),  $D_0$  is the diffusion coefficient ( $\text{cm}^2\cdot\text{s}^{-1}$ ),  $C^0$  is the bulk concentration in ( $\text{mol}\cdot\text{cm}^{-3}$ )  $v$  is the scan rate ( $\text{V}\cdot\text{s}^{-1}$ ),  $R$  is the Gas constant ( $\text{J}\cdot\text{K}^{-1}\text{mol}^{-1}$ ) and  $T$  is temperature (K). We modified the size of the WE area from  $9\text{ mm}^2$  to one size smaller  $7\text{ mm}^2$  and two sizes larger  $13\text{ mm}^2$  and  $20\text{ mm}^2$ . The photographs of the devices are shown in figure 24a-d. The devices were tested using a sample of  $0.1\text{ M}$  phosphate buffer at pH 7.0. On the CV overlay (Figure 24e), we observe an increase in the size of the redox peaks as the

area of the WE increases. The plot (Figure 24f-g) has a linear response with an  $R^2$  value of 0.9967 for the current intensity of the oxidation peak and 0.9902 for the current intensity of the reduction peak. The results confirmed the hypothesis that increasing the WE area would increase the measured current and following the established (eq 3). The optimized area selected based on the results was the largest area,  $20 \text{ mm}^2$ .

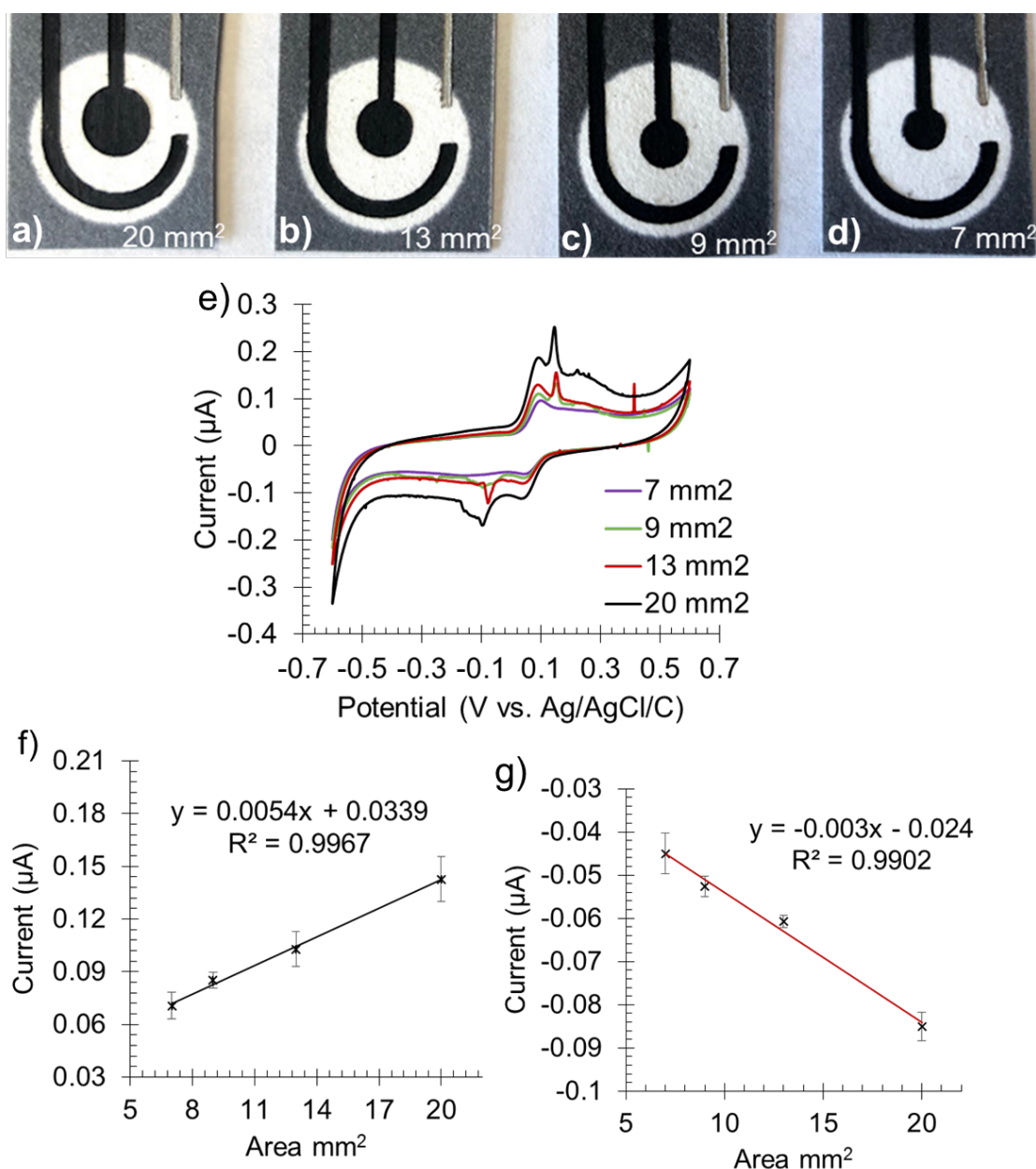


Figure 24. a-d) Photographs of devices with area of WE varying from  $7 \text{ mm}^2$  to  $20 \text{ mm}^2$ . e) CVs collected on the different devices showing an increase in current with the increasing area of the WE. f) Calibration curve of oxidation peaks. g) Calibration curve of reduction peaks.

### 6.3 Optimization of the Method: Conditioning Step

The combination of Grade 2 (P2) filter paper and WE area of 20 mm<sup>2</sup>, resulted in an increase in the peak definition and current intensity. Now we needed to increase the accuracy of peaks observed on the paper-based devices with our method. In a study reported by Motin *et al.* the electrochemical oxidation of catechol (a derivative of quinone) in the presence of sulfanilic acid was studied at different pH.<sup>61</sup> In this study, they used a GCE to run their CVs, the potential range at which they did their test was from 2 V to - 0.5 V.<sup>61</sup> In all previous tests we ran the CVs with potential range between 0.6 V to - 0.6 V. Using a sample of 0.1 M phosphate buffer at pH 7.0, we ran CVs that start at various potentials between 0.6 V and 1 V. The overlay of the CVs is shown in figure 25a, an increase in the current is observed as the starting potential increases. There is no change in peak current when we start at a potential of 0.7 V instead of 0.6 V, however starting at a potential of 0.8 V generated an increase in the peak current. The increase continues as the starting potential is changed to 0.9 V and 1V. To determine the initial potential at which the redox couple would reach the highest current, we started the CVs with an increment in potential of 0.05 V. The overlay of these CVs (Figure 25b), shows that changing the start potential from 0.60V to 0.85 V has a great effect on the current. The peak current remains, however the same when changing the start in potential from 0.85V to 1 V.

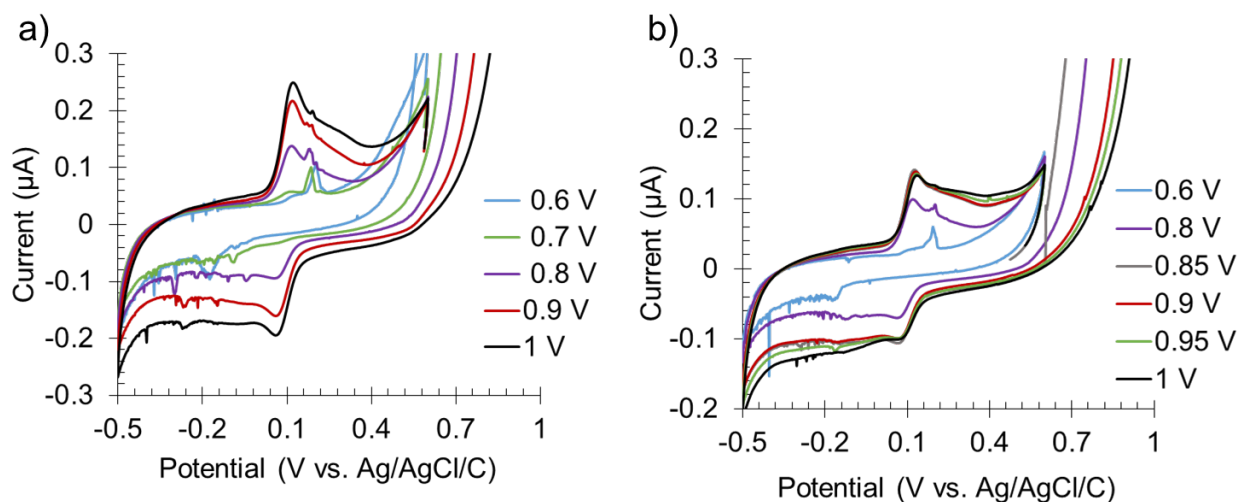


Figure 25. a) CVs starting between 0.6 V and 1 V with 100-mV increments. b) CVs starting between 0.6 V and 1 V with 50-mV increments.

The change in current confirmed that the addition of a conditioning oxidative potential enhances the redox activity of the pH-sensitive electroactive species on the electrode. We hypothesize that starting at a higher potential allowed for oxidation of the quinone at the surface of the electrode which would then be reduced and oxidized to display redox peaks with a greater current. Due to variation between devices (data not shown), 1V was selected as the optimal starting potential, as this ensures that every device will oxidize the maximum species which will then show sharp and well-defined redox peaks.

#### 6.4 Conclusion

The design of the paper-based device was optimized and a conditioning step to increase the pH-sensing ability of the method was added. Different filter papers were used to fabricate the devices and Grade 2 (P2) yielded an increase in peak definition and a higher percentage of devices showing peaks compared to other filter papers. Working electrodes with greater area (9 mm<sup>2</sup> to 20 mm<sup>2</sup>) increased the intensity of current. Starting the CV at a higher potential (1 V) helped form pH-sensitive species on the surface of the electrode. The next chapter will focus on applying the optimized design and method to measure different samples over the full pH scale.

## CHAPTER 7. DETERMINATION OF PH WITH OPTIMIZED DEVICE AND METHOD

### 7.1 Measuring pH in Various Buffers and Solutions

In the previous chapter, we successfully optimized the design of the PBD and the method for measuring pH. To evaluate the performance of the optimized method we tested various buffers. The list of buffer solutions tested are shown in table 2. As mentioned in previous chapters, measuring partially acidic pH is of importance for the future application of the PBD in oral care. To test acidic pH we used citrate buffer, which has a pH ranging from 2 to 5. We were able to obtain good results with low pH solutions using the conditioning step. The overlay of the CVs of citrate buffer at different pH (Figure 26a) shows well-defined redox peaks, with a clear shift in the redox peaks as the pH increases. A calibration curve of the reduction potential peaks (Figure 26b) shows a great linear response with an  $R^2$  value of 0.9987.

*Table 2. List of buffer solutions and pH range.*

Solutions	pH Range	Composition
HCl / NaOH	1 - 5	HCl / NaOH
Citrate buffer	2 - 5	Citric acid / Sodium citrate / KCl
Mcllvaine buffer	3 - 8	Citric acid / $\text{Na}_2\text{HPO}_4$
Phosphate buffer	5 - 9	$\text{NaH}_2\text{PO}_4$ / $\text{Na}_2\text{HPO}_4$

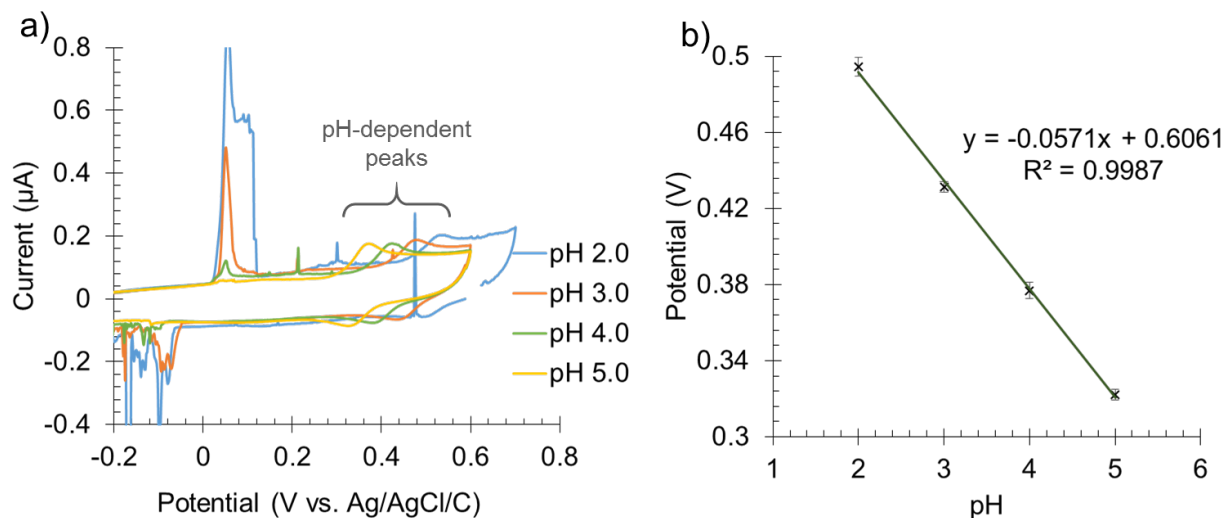


Figure 26. a) Overlay of 0.1 M Citrate buffer with pH varying from 2 to 5. b) Calibration curve of reduction peaks potential over the average of two cycles.

To examine the robustness of the improved method, we used the same devices to test additional buffer solutions. Paper-based devices A and B were used to test the following solutions: HCl/NaOH solutions, citrate buffer solutions, McIlvaine buffer solutions, and phosphate buffer solutions. The potential of the reduction peaks of each CV were collected and plotted (Figure 27). Both devices A and B have good linear responses, most of the solutions had an  $R^2$  value of 0.98 or greater on the same device. We could not achieve such repeatable results on our devices prior to optimization. The HCl/NaOH solutions on device A had a poor linear response (Figure 27a purple), we believe that the poor results were due device A being used for more than 30 CVs before being used to run the HCl/NaOH solutions. Despite the poor linear response, we observe a shift in redox peaks as the pH increased. While overlaying the data of all the different buffers, we observed that the potential values were not the same for different solutions at same pH. Phosphate buffer and McIlvaine buffer showed similar results for pH 5 to 8. We hypothesized this could be due to the sodium phosphate dibasic ( $\text{Na}_2\text{HPO}_4$ ) common in both solutions. Citrate Buffer and HCl/NaOH displayed the similar results for pH 2 to 5. We hypothesized this could be due to  $\text{Na}^+$  and  $\text{Cl}^-$  ions present in both solutions. These results made it necessary to study the effect of certain ions in solutions.

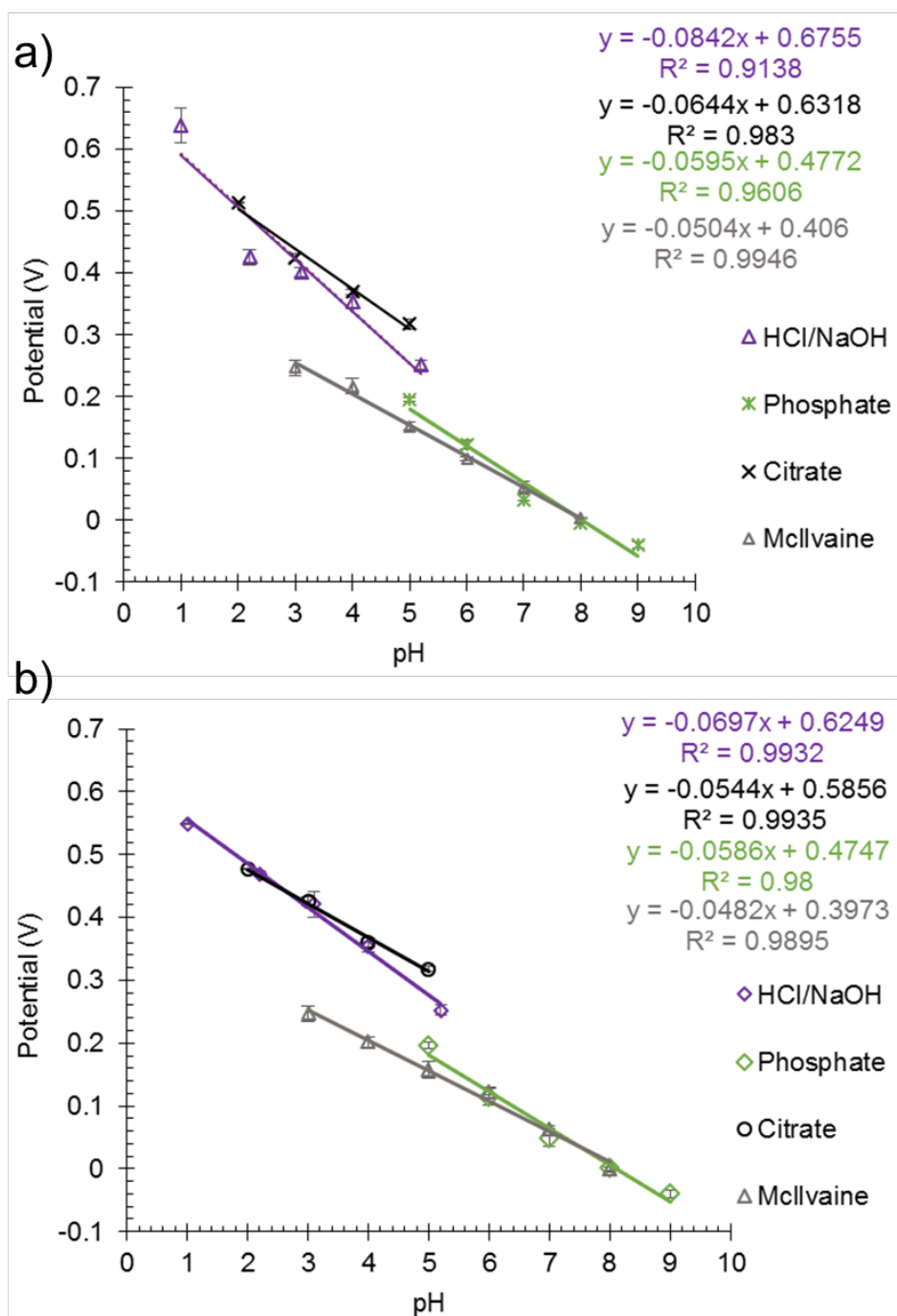


Figure 27. a) Calibration curves of HCl/NaOH solutions with pH ranging from 1 to 5, citrate buffers with pH ranging from 2 to 5, Mcllvaine buffers with pH ranging from 3 to 8, and phosphate buffers with pH ranging from 5 to 9 tested on device A. b) Calibration curves of the same solutions tested on device B.



## 7.2 Effect of Adding Sodium Chloride to pH Solutions

To study the effect that adding sodium chloride to solutions had on pH-sensing PBD, we spiked Mcllvaine and phosphate buffer with NaCl. We then ran CVs of the solutions made with sodium chloride on a new paper-based device (device C). We also measured the citrate buffer again on device C as a control. The potentials of all the reduction peaks were collected over two cycles and the averages were plotted. Figure 28 is the overlay comparing all the solutions from device B to citrate buffer and Mcllvaine and phosphate buffer containing sodium chloride on device C. After adding 0.1 M NaCl to the buffer solutions we observe an alignment of the Mcllvaine and the phosphate buffer containing NaCl with the HCl/NaOH and citrate buffer curve. The solutions with the same pH now have the same results (potential values) due to the addition of sodium chloride.

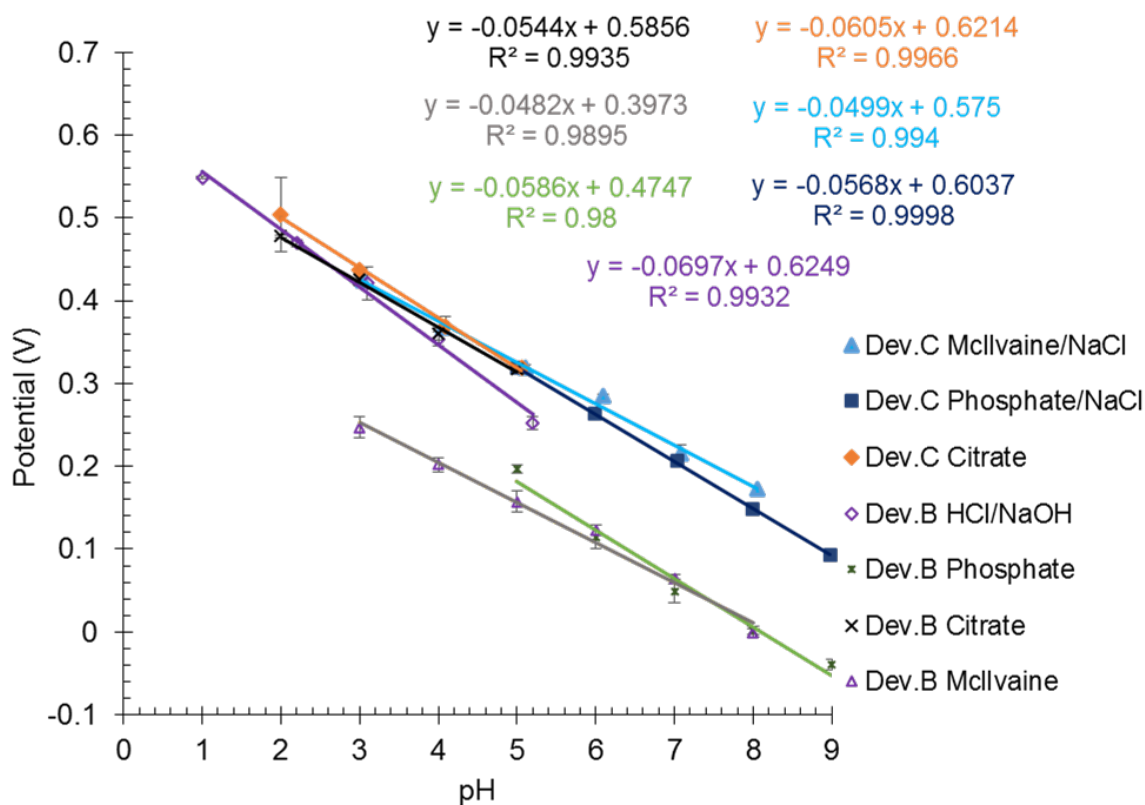


Figure 28. Overlay of plots with and without NaCl

### 7.3 Measuring pH from 0 to 13

#### 7.3.1 HCl/NaOH

To reach the full pH range, solutions using HCl and NaOH with pH ranging from 1 to 13 were made and tested. The potentials of the reduction peaks for all CVs were plotted and a linear response with an  $R^2$  value of 0.9979 was observed (Figure 29). The observed results confirm that there is presence of electroactive elements that are pH-dependent on the surface of the PBD pH sensor and that method can successfully quantify pH over the full range.

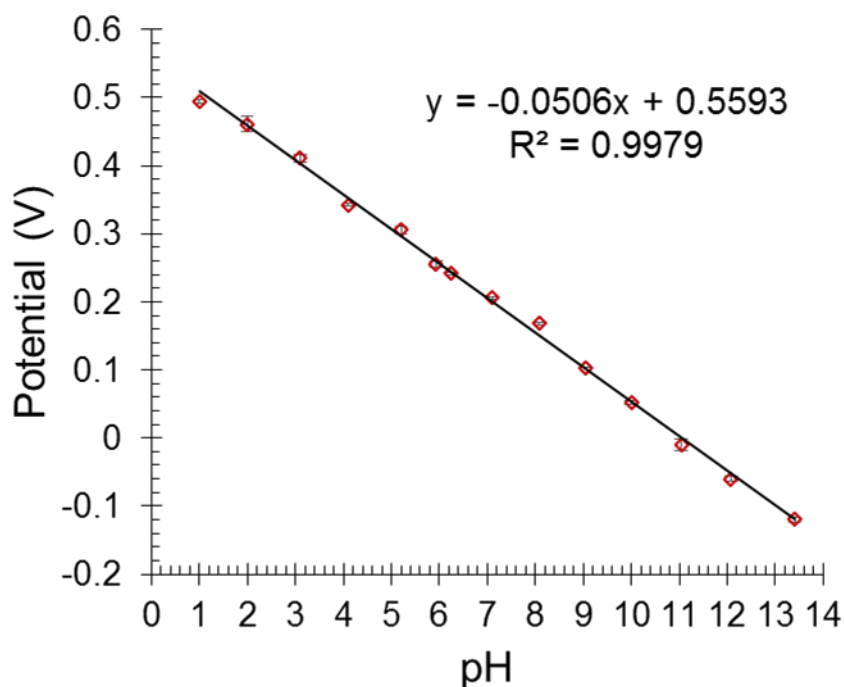


Figure 29. Calibration curve of potentials of the reduction peaks versus pH on the PBD in solutions of HCl and NaOH prepared with pH ranging from 1 to 13.

#### 7.3.2 Standard pH Solutions

To determine if the results obtained from the measurement of the full range of pH on HCl and NaOH pH solutions could be repeated, we tested commercial pH standards with pH ranging from 1 to 12. The test was first done in the standard solutions as they were. The potentials of the reduction peaks were plotted (Figure 30a) all data points are not aligned, as the results for pH 5, 6, and 7 formed a separate “trend-line”. Standard solutions are made with different compositions to ensure a stable pH for traceable results. To confirm our previous hypothesis that a certain amount of NaCl was needed, we added 0.1 M NaCl to all the standard solutions and tested them again.

The potentials of reduction peaks of CVs were plotted (Figure 30b). The results for the solutions at pH 5, 6 and 7 are now aligned with other standards and we could observe a great linear correlation with an  $R^2$  value of 0.9977. Additionally, the standard solution at pH 8 could not be detected before NaCl addition due to some interferences with other electroactive species in the solution, but with NaCl, we were able to observe redox peaks at the expected potential for a pH 8 solution. These results thus confirm that using the method developed for our paper-based devices, pH can be successfully measured.

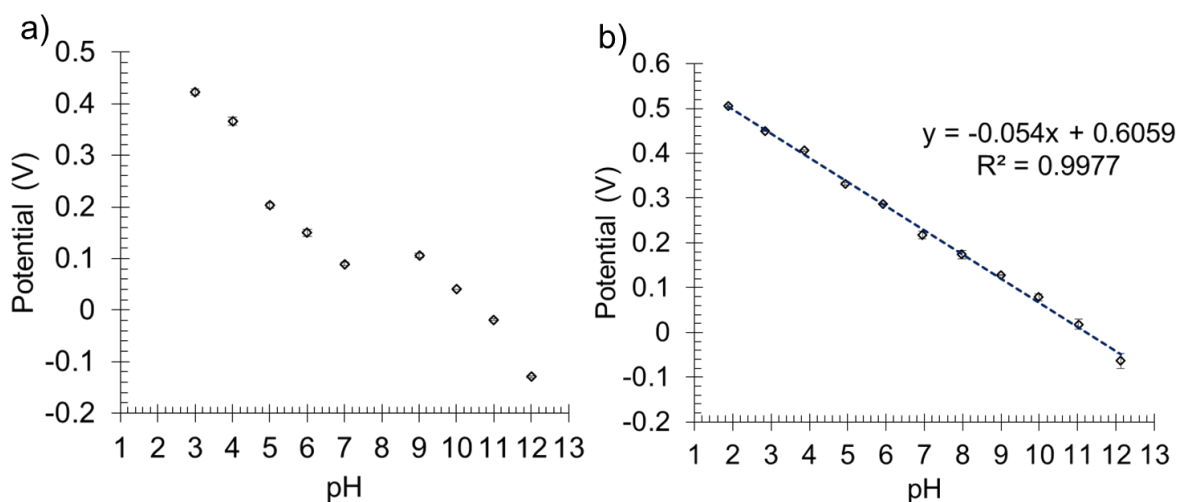


Figure 30. Plots of potentials of the reduction peaks versus pH on the PBD in standard pH solutions with pH ranging from 1 to 12, a) without NaCl added and b) with 0.1M NaCl added.

#### 7.4 Repeatability of Method on PBDs

The repeatability of the optimized method using paper-based device to measure pH was assessed. Two different students conducted a series of tests on four paper-based devices, I and an undergraduate student assessed the repeatability and robustness of our method. The undergraduate student prepared solutions of McIlvaine buffer with pH ranging from 3 to 8 and ran CVs on three PBDs devices E4, E5 and E6. Using the same solutions prepared by the undergraduate student, I ran CVs on PBD device E170. Figure 31 is the overlay of calibration curves for all four devices, and both users. The observed linear responses have  $R^2$  values around 0.98 – 0.99 for both the oxidation and the reduction peaks. The coefficients are slightly lower than previous results in this chapter due to the solution at pH 4 which was slightly off for all devices. All four trials on independent devices present the same trends even when fabricated and used by two different users,

and with one month separating the two sets of tests. These results confirm that the method developed on our electrochemical paper-based devices is robust and can produce repeatable results.

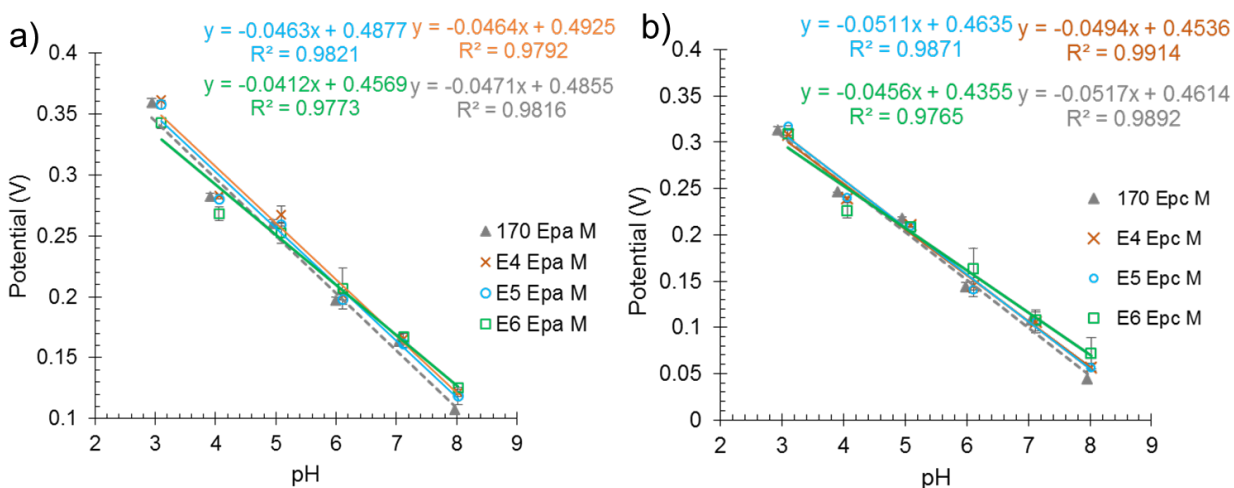


Figure 31. Repeatability tests on four different PBDs performed by two users. a) Overlay of calibration curves using the potentials of oxidation peaks. b) Overlay of calibration curves using the potentials of reduction peaks

### 7.5 pH Measurement of Artificial saliva

The future goal of this project is to use the developed pH-sensor PBD to measure the pH of plaque on the surface of the teeth of patients, to mimic the environment of the mouth by measuring the pH of artificial saliva. We prepared some artificial saliva according to the composition listed in table 3.<sup>12,47</sup> We performed CVs in the artificial saliva with pH ranging from 3 to 8 on two PBDs, as the pH of plaque in dental cavities is below the critical pH value of 5.5.<sup>12</sup> The results from plotting the potentials of the reduction peaks (average over two CV cycles) shows a good linear correlation (Figure 32). Some data points on both devices have a standard deviation larger than desired, we hypothesize that the electroactive species from the different chemicals in the composition of the saliva could have caused subsequent cycles to differ more from one another than when using buffers. These results suggest that using our method on the PBDs could allow for pH measurements in real saliva.

Table 3. Composition list for artificial saliva (AFNOR standard S90-701; Association Française de Normalisation—French Standardization Association)<sup>12,47</sup>

Chemicals	Concentration	mmol/L
Na <sub>2</sub> HPO <sub>4</sub>	0.260 g/l	1 mM
KH <sub>2</sub> PO <sub>4</sub>	0.200 g/l	1.5 mM
NaHCO <sub>3</sub>	1.500 g/l	18 mM
KSCN	0.330 g/l	3 mM
NaCl	6.700 g/l	115 mM
KCl	1.200 g/l	16 mM

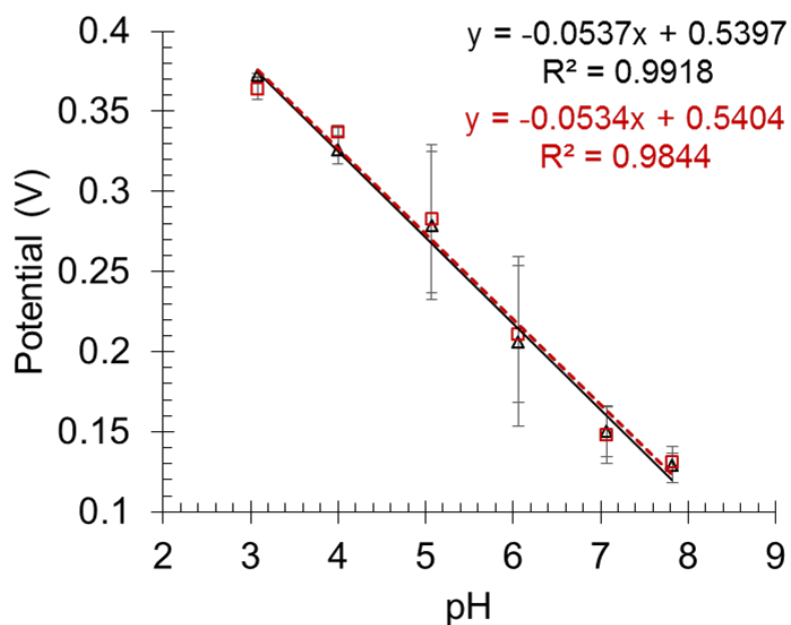


Figure 32. Calibration curve the potential of reduction peaks of two devices (black = device 1, red = device 2) in artificial saliva with the pH ranging from 3 to 8.

## 7.6 Conclusion

In this chapter, the optimized design and method was successfully used to measure pH in various solutions. The PBD pH-sensing helped determine pH of various buffers listed in table 2 with pH ranging from 1 to 9. The results obtained from various buffers lead to the need to study

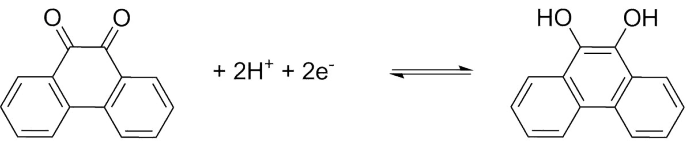
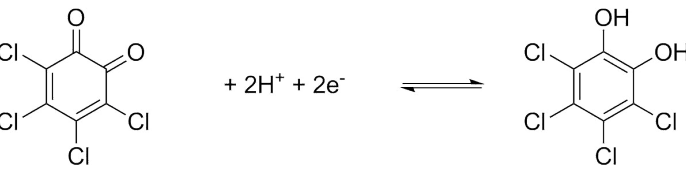
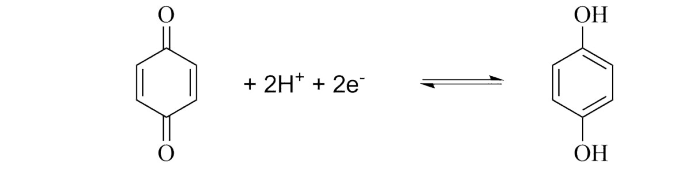
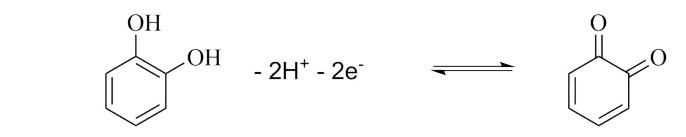
the effect of certain ions in solutions. Adding sodium chloride to solutions acted as an ion adjuster and allowed the redox peaks for having similar potentials for solutions of same pH. The pH range from 1 to 13 was successfully assessed using HCl/NaOH solutions. To test other samples over a wide pH range commercial standards with pH ranging from 1 to 12 was measured. Artificial saliva with pH ranging from 3 to 8 was successfully measured, suggesting that the developed paper-based pH-sensor could be applied to measure the pH of real saliva and then guide oral preventative care.

## CHAPTER 8. FUTURE WORK

### 8.1 Preliminary Work on Identifying the pH-sensing Species

While developing the electrochemical pH-sensing PBD, we hypothesized that the pH-sensitive species present at the surface of the electrode was *ortho*-quinone, however this would need to be further confirmed. To start exploring which oxo-group(s) is responsible for detecting pH on the surface of the electrodes painted on the PBDs, we tested various commercially available derivatives of quinone. The redox reaction of the quinone derivatives tested is shown in table 4.

Table 4. List of quinone derivatives and their associated reduction reactions.

	9,10-phenanthrenequinone
	tetrachloro- <i>o</i> -benzoquinone
	1,4-benzoquinone
	catechol $\rightleftharpoons$ <i>o</i> -benzoquinone

We tested the quinone derivatives that were close to *ortho*-quinone because it is not commercially available. The derivatives were tested at two different pH (2 and 7) on the paper-based devices, the CVs for 9,10-phenanthrenequinone (PAQ), tetrachloro-*o*-benzoquinone (TCBQ) and 1,4-benzoquinone (p-Ben) are shown in figure 33. The un-spiked solution at pH 2 is a solution of citrate buffer which is overlaid using the secondary y-axis, the redox couple for pH 2 is showing around the potential of 0.40 V (Figure 33a). When comparing the un-spiked to the solutions spiked with quinone derivatives we observe different couples of redox peaks that have potentials more

negative than the un-spiked. The un-spiked at pH 7 is in a solution of phosphate buffer and has a redox couple that is seen around potential 0.06 V (Figure 33b). The CV of the un-spiked overlaid with the solutions spiked with quinone derivatives also shows a different redox couple with potential that is more negative than the un-spiked. The results at both pH show that when the solution is spiked with PAQ, TCBQ and p-benzoquinone the redox couples are different from the un-spiked thus confirming that neither of them is the species present on the surface of the electrodes painted on the PBDs. Since the spiked solutions are all tested on PBDs we should indeed always observe the “unknown” pH-sensing peaks along with the “spiked” peaks. The test was also run using catechol, the reduced form of o-benzoquinone. The derivative was run in solutions at pH 2 and pH 7, the CVs are overlaid in figure 34. The CV of the un-spiked and the catechol at pH 2 have a redox couple that match, but the catechol has a second reduction peak (Figure 34a). At pH 7 the un-spiked and the catechol have the same redox couple (Figure 34b). Based on these results there could be two derivatives of quinone present on the surface of the electrodes painted on the PBDs. We hypothesize that the oxidation reaction used in PBD pH-sensing could correspond to the oxidation of catechol and the reduction used in PBD pH-sensing could correspond to the reduction of p-Benzoquinone. More experiment with other analytical characterizing techniques such as mass spectrometry and NMR will be needed to positively identify the pH-sensing elements.

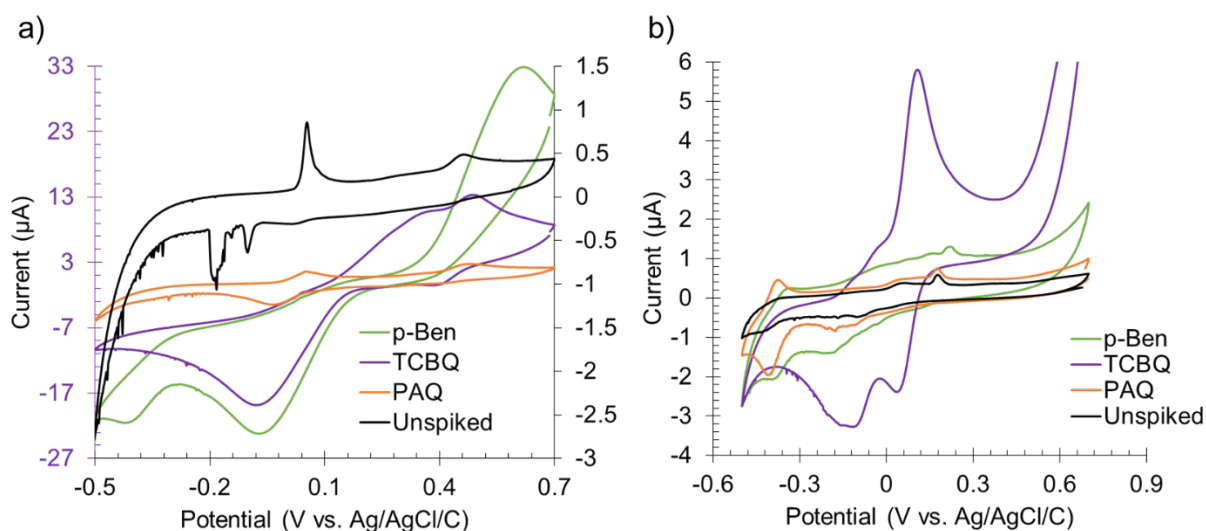


Figure 33. CVs of 9,10-Phenanthrenequinine (PAQ), Tetrachloro-o-Benzoquinone (TCBQ) and 1,4-Benzoquinone (p-Ben) in a) citrate buffer at pH 2 and b) phosphate buffer at pH 7



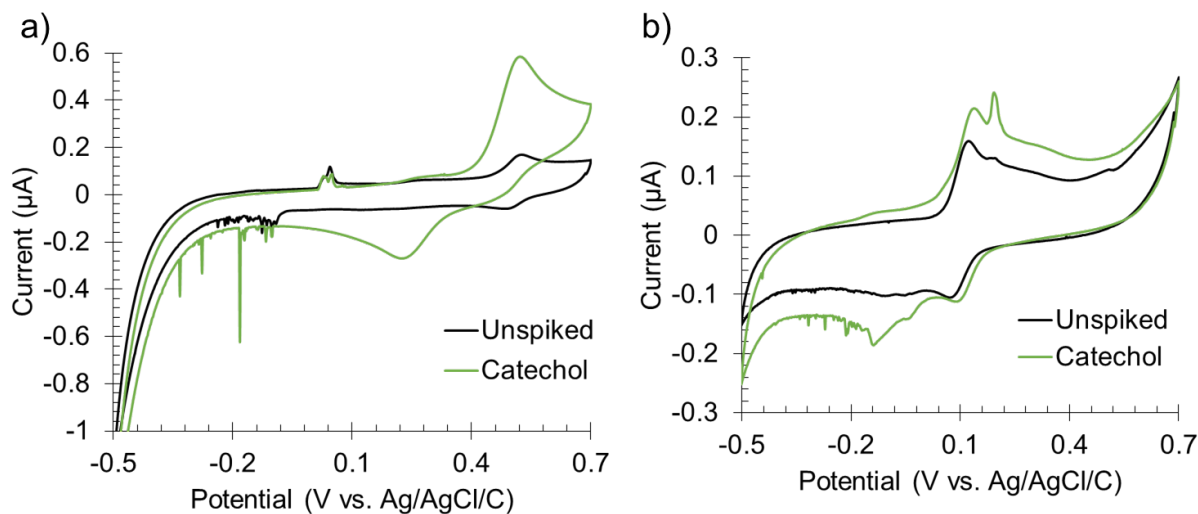


Figure 34. CVs of catechol in a) citrate buffer at pH 2 and b) phosphate buffer at pH 7

## 8.2 Real Samples of Food and Beverages

Measuring the pH of food and beverages is important for quality control as well as, in processes used in the food industry such as for water absorption, emulsification, and gelation of different protein sources.<sup>8</sup> the pH of food and beverages can also influence the pH of saliva which inspired the need to test such samples and also allows for the assessment of the pH-sensor PBD in variable complex matrices. We will test samples such as soda, orange juices, milk for pH-sensing in “real” unbuffered samples with the optimized PBD. As a first trial, we tested a sample of distilled white vinegar, for which a pH of 2.4 was measured using the pH meter. The CVs were run on one PBD, and the CVs are overlaid in figure 35. The difference between cycle 1 and 2 from the same run, showed different results and the peaks believed to correspond to the pH-sensing peaks at 370 mv and 320 mv for oxidation and reduction respectively, do not correlate with a pH of 2.4 when using previous calibration curve from figure 29. Future work will be needed on other food and beverages to determine if the method developed for our PBDs can measure the pH on these types of samples and what optimizations or adjustments might be necessary.

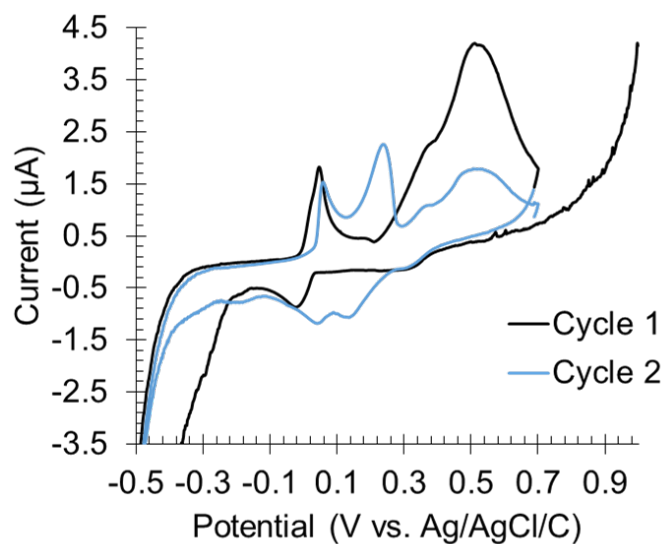


Figure 35. CV overlay of distilled white vinegar with a pH of 2.4

### 8.3 Apply PBD pH Sensor to Real Saliva and Bacteria

Being able to measure pH of real saliva and of bacteria will be needed to work towards the future goals of this project: to apply the pH-sensor PBD to analyze the pH in bacterial biofilms formed on teeth (or plaque) as it can be indicative of conditions leading to the formation of cavities. The work that will be done would involve collaborations with the dental school to collect samples of saliva from their patient, we will then analyze the pH of the samples using the PBDs. We will also assess pH in bacterial biofilm that we will culture in the lab first with *E.coli* K12 non pathogen and the typical mouth bacterial strains such as mutants *streptococci* and *Lactobacilli*.<sup>62</sup>

## CONCLUSION

This thesis described the successful development of a low-cost, flexible and portable electrochemical microfluidic paper-based analytical device for pH-sensing. Different optimization methods were performed to enhance the definition of redox peaks on the CVs. They included chemical modification of the electrode by adsorption of sodium carbonate and modification of the surface of the electrode to form more functional groups by different plasma treatments. The optimization of the design of the paper-based device and the addition of a conditioning step improved the definition of the redox peaks and increased the precision of the method. Various solutions over a wide range of pH (1 to 13) were successfully tested. The addition of sodium chloride to solutions improved the accuracy of pH measurements. The pH of artificial saliva at various pH values in the cavity-prone range was measured and showed the applicability of this paper-based electrochemical pH sensor for future pH measurements in real saliva and bacterial biofilms.

## REFERENCES

1. Baron, J. H., The Discovery of Gastric Acid. *Gastroenterology* **1979**, *76* (5), 1056-1064.
2. G. L. Miessler, D. A. T., *Inorganic Chemistry*. 3 rd ed.; Prentice Hall: 1999; p 632.
3. Salvo, P.; Melai, B.; Calisi, N.; Paoletti, C.; Bellagambi, F.; Kirchhain, A.; Trivella, M.; Fuoco, R.; Di Francesco, F., Graphene-based devices for measuring pH. *Sensors Actuators B: Chemical* **2017**.
4. An Education Poster Of PH Scale. [www.vecteezy.com/vector-art/296166-an-education-poster-of-ph-scale](http://www.vecteezy.com/vector-art/296166-an-education-poster-of-ph-scale) (accessed June 28th 2019).
5. Lafitte, V. G.; Wang, W.; Yashina, A. S.; Lawrence, N. S., Anthraquinone–ferrocene film electrodes: utility in pH and oxygen sensing. *Electrochemistry Communications* **2008**, *10* (12), 1831-1834.
6. Lu, M.; Compton, R. G., Voltammetric pH sensing using carbon electrodes: glassy carbon behaves similarly to EPPG. *Analyst* **2014**, *139* (18), 4599-4605.
7. Lu, M.; Compton, R. G., Voltammetric pH sensor based on an edge plane pyrolytic graphite electrode. *Analyst* **2014**, *139* (10), 2397-2403.
8. Karastogianni, S.; Grousi, S.; Sotiropoulos, S., pH: Principles and Measurement. *The Oxford: Academic Press. Encyclopedia of Food and Health* **2016**, 333-8.
9. Mettler Toledo Sven Compact modular pH meter/ion sensor. [www.mt.com](http://www.mt.com) (accessed July 15th 2019).
10. Oakton™ pHTestr™ Waterproof Pocket pH Testers. [www.fishersci.com](http://www.fishersci.com) (accessed July 15th 2019).
11. Azzota Corp Multi Parameter Ion Meter. [www.fishersci.com](http://www.fishersci.com) (accessed July 15th 2019).
12. Chaisiwamongkhol, K.; Batchelor-McAuley, C.; Compton, R. G., Amperometric micro pH measurements in oxygenated saliva. *Analyst* **2017**, *142* (15), 2828-2835.
13. Zhang, X.; Ogorevc, B.; Wang, J., Solid-state pH nanoelectrode based on polyaniline thin film electrode deposited onto ion-beam etched carbon fiber. *Analytica chimica acta* **2002**, *452* (1), 1-10.
14. Wencel, D.; Abel, T.; McDonagh, C., Optical chemical pH sensors. *Analytical chemistry* **2013**, *86* (1), 15-29.
15. Zhang, J.; Zhou, L., Preparation and Optimization of Optical pH Sensor Based on Sol-Gel. *Sensors* **2018**, *18* (10), 3195.
16. Gotor, R. I.; Ashokkumar, P.; Hecht, M.; Keil, K.; Rurack, K., Optical pH sensor covering the range from pH 0–14 compatible with mobile-device readout and based on a set of rationally designed indicator dyes. *Analytical chemistry* **2017**, *89* (16), 8437-8444.
17. Seitz, W. R., Optical sensors for clinical applications. *Journal of Clinical Laboratory Analysis* **1987**, *1* (3), 313-316.
18. Duroux, P.; Emde, C.; Bauerfeind, P.; Francis, C.; Grisel, A.; Thybaud, L.; Armstrong, D.; Depeursinge, C.; Blum, A., The ion sensitive field effect transistor (ISFET) pH electrode: a new sensor for long term ambulatory pH monitoring. *Gut* **1991**, *32* (3), 240-245.
19. Rani, R. A.; Sidek, O. In *ISFET pH sensor characterization: towards biosensor microchip application*, 2004 IEEE Region 10 Conference TENCON 2004., IEEE: 2004; pp 660-663.

20. Thorogood, C. A.; Wildgoose, G. G.; Jones, J. H.; Compton, R. G., Identifying quinone-like species on the surface of graphitic carbon and multi-walled carbon nanotubes using reactions with 2, 4-dinitrophenylhydrazine to provide a voltammetric fingerprint. *New Journal of Chemistry* **2007**, *31* (6), 958-965.
21. Thorogood, C. A.; Wildgoose, G. G.; Crossley, A.; Jacobs, R. M.; Jones, J. H.; Compton, R. G., Differentiating between ortho-and para-quinone surface groups on graphite, glassy carbon, and carbon nanotubes using organic and inorganic voltammetric and X-ray photoelectron spectroscopy labels. *Chemistry of Materials* **2007**, *19* (20), 4964-4974.
22. Beitollahi, H.; Garkani Nejad, F., Graphene oxide/ZnO nano composite for sensitive and selective electrochemical sensing of levodopa and tyrosine using modified graphite screen printed electrode. *Electroanalysis* **2016**, *28* (9), 2237-2244.
23. Gong, Z.; Zhang, G.; Wang, S., Electrochemical Reduction of Oxygen on Anthraquinone/Carbon Nanotubes Nanohybrid Modified Glassy Carbon Electrode in Neutral Medium. *Journal of Chemistry* **2013**, *2013*, 1-9.
24. McDermott, M. T.; McCreery, R. L., Scanning tunneling microscopy of ordered graphite and glassy carbon surfaces: electronic control of quinone adsorption. *Langmuir* **1994**, *10* (11), 4307-4314.
25. Sinha, S.; Rathore, R.; Sinha, S.; Sharma, R.; Mukhiya, R.; Khanna, V. In *Modeling and simulation of ISFET microsensor for different sensing films*, ISSS International Conference on Smart Materials, Structures and Systems, 2014.
26. Park, K.-Y.; Choi, S.-B.; Lee, M.; Sohn, B.-K.; Choi, S.-Y., ISFET glucose sensor system with fast recovery characteristics by employing electrolysis. *Sensors and Actuators B: Chemical* **2002**, *83* (1-3), 90-97.
27. Galdino, F. v. E.; Smith, J. P.; Kwamou, S. I.; Kampouris, D. K.; Iniesta, J.; Smith, G. C.; Bonacin, J. A.; Banks, C. E., Graphite screen-printed electrodes applied for the accurate and reagentless sensing of pH. *Analytical chemistry* **2015**, *87* (23), 11666-11672.
28. Guinovart, T.; Valdés-Ramírez, G.; Windmiller, J. R.; Andrade, F. J.; Wang, J., Bandage-Based Wearable Potentiometric Sensor for Monitoring Wound pH. *Electroanalysis: An International Journal Devoted to Fundamental* **2014**, *26* (6), 1345-1353.
29. Bandodkar, A. J.; Hung, V. W.; Jia, W.; Valdés-Ramírez, G.; Windmiller, J. R.; Martinez, A. G.; Ramírez, J.; Chan, G.; Kerman, K.; Wang, J., Tattoo-based potentiometric ion-selective sensors for epidermal pH monitoring. *Analyst* **2013**, *138* (1), 123-128.
30. Nyein, H. Y. Y.; Gao, W.; Shahpar, Z.; Emaminejad, S.; Challa, S.; Chen, K.; Fahad, H. M.; Tai, L.-C.; Ota, H.; Davis, R. W., A wearable electrochemical platform for noninvasive simultaneous monitoring of Ca<sup>2+</sup> and pH. *ACS nano* **2016**, *10* (7), 7216-7224.
31. Bandodkar, A. J.; Wang, J., Non-invasive wearable electrochemical sensors: a review. *Trends in biotechnology* **2014**, *32* (7), 363-371.
32. Rahimi, R.; Ochoa, M.; Parupudi, T.; Zhao, X.; Yazdi, I. K.; Dokmeci, M. R.; Tamayol, A.; Khademhosseini, A.; Ziaie, B., A low-cost flexible pH sensor array for wound assessment. *Sensors Actuators B: Chemical* **2016**, *229*, 609-617.
33. Nag, A.; Mukhopadhyay, S. C.; Kosel, J., Wearable flexible sensors: A review. *IEEE Sensors Journal* **2017**, *17* (13), 3949-3960.
34. Maiolo, L.; Mirabella, S.; Maita, F.; Alberti, A.; Minotti, A.; Strano, V.; Pecora, A.; Shacham-Diamand, Y.; Fortunato, G., Flexible pH sensors based on polysilicon thin film transistors and ZnO nanowalls. *Applied Physics Letters* **2014**, *105* (9), 093501.

35. Nakata, S.; Arie, T.; Akita, S.; Takei, K., Wearable, flexible, and multifunctional healthcare device with an ISFET chemical sensor for simultaneous sweat pH and skin temperature monitoring. *ACS sensors* **2017**, *2* (3), 443-448.
36. Lopez-Ruiz, N.; Curto, V. F.; Erenas, M. M.; Benito-Lopez, F.; Diamond, D.; Palma, A. J.; Capitan-Vallvey, L. F., Smartphone-based simultaneous pH and nitrite colorimetric determination for paper microfluidic devices. *Analytical chemistry* **2014**, *86* (19), 9554-9562.
37. Mettakoonpitak, J.; Boehle, K.; Nantaphol, S.; Teengam, P.; Adkins, J. A.; Srisa-Art, M.; Henry, C. S., Electrochemistry on Paper-based Analytical Devices: A Review. *Electroanalysis* **2016**, *28* (7), 1420-1436.
38. Martinez, A. W.; Phillips, S. T.; Butte, M. J.; Whitesides, G. M., Patterned paper as a platform for inexpensive, low-volume, portable bioassays. *Angewandte Chemie International Edition* **2007**, *46* (8), 1318-1320.
39. Deiss, F.; Funes-Huacca, M. E.; Bal, J.; Tjhung, K. F.; Derda, R., Antimicrobial susceptibility assays in paper-based portable culture devices. *Lab on a Chip* **2014**, *14* (1), 167-171.
40. Deiss, F.; Matochko, W. L.; Govindasamy, N.; Lin, E. Y.; Derda, R., Flow-through synthesis on teflon-patterned paper to produce peptide arrays for cell-based assays. *Angewandte Chemie International Edition* **2014**, *53* (25), 6374-6377.
41. Deiss, F.; Yang, Y.; Matochko, W. L.; Derda, R., Heat-enhanced peptide synthesis on Teflon-patterned paper. *Organic & biomolecular chemistry* **2016**, *14* (22), 5148-5156.
42. Dungchai, W.; Chailapakul, O.; Henry, C. S., Electrochemical detection for paper-based microfluidics. *Analytical chemistry* **2009**, *81* (14), 5821-5826.
43. Nie, Z.; Deiss, F.; Liu, X.; Akbulut, O.; Whitesides, G. M., Integration of paper-based microfluidic devices with commercial electrochemical readers. *Lab on a Chip* **2010**, *10* (22), 3163-3169.
44. Rattanarat, P.; Dungchai, W.; Cate, D.; Volckens, J.; Chailapakul, O.; Henry, C. S., Multilayer paper-based device for colorimetric and electrochemical quantification of metals. *Analytical chemistry* **2014**, *86* (7), 3555-3562.
45. Dossi, N.; Toniolo, R.; Pizzariello, A.; Impellizzieri, F.; Piccin, E.; Bontempelli, G., Pencil-drawn paper supported electrodes as simple electrochemical detectors for paper-based fluidic devices. *Electrophoresis* **2013**, *34* (14), 2085-2091.
46. Dossi, N.; Toniolo, R.; Piccin, E.; Susmel, S.; Pizzariello, A.; Bontempelli, G., Pencil-Drawn Dual Electrode Detectors to Discriminate Between Analytes Comigrating on Paper-Based Fluidic Devices but Undergoing Electrochemical Processes with Different Reversibility. *Electroanalysis* **2013**, *25* (11), 2515-2522.
47. Elagli, K.; Traisnel, M.; Hildebrand, H., Electrochemical behaviour of titanium and dental alloys in artificial saliva. *Electrochimica acta* **1993**, *38* (13), 1769-1774.
48. Lahav, M.; Katz, E.; Willner, I., A Covalently Linked Quinone-Ferrocene Monolayer-Electrode: A pH Sensor with an Internal Reference. *Electroanalysis: An International Journal Devoted to Fundamental Practical Aspects of Electroanalysis* **1998**, *10* (17), 1159-1162.
49. Banks, C. E.; Compton, R. G., New electrodes for old: from carbon nanotubes to edge plane pyrolytic graphite. *Analyst* **2006**, *131* (1), 15-21.

50. Schreurs, J.; Van den Berg, J.; Wonders, A.; Barendrecht, E., Characterization of a glassy-carbon-electrode surface pretreated with rf-plasma. *Recueil des Travaux Chimiques des Pays-Bas* **1984**, *103* (9), 251-259.
51. Schweigert, N.; Zehnder, A. J.; Eggen, R. I., Chemical properties of catechols and their molecular modes of toxic action in cells, from microorganisms to mammals: minireview. *Environmental microbiology* **2001**, *3* (2), 81-91.
52. Hrbac, J.; Halouzka, V.; Trnkova, L.; Vacek, J., eL-Chem Viewer: A freeware package for the analysis of electroanalytical data and their post-acquisition processing. *Sensors* **2014**, *14* (8), 13943-13954.
53. Kano, K.; Uno, B., Surface-redox reaction mechanism of quinones adsorbed on basal-plane pyrolytic graphite electrodes. *Analytical Chemistry* **1993**, *65* (8), 1088-1093.
54. Streeter, I.; Leventis, H. C.; Wildgoose, G. G.; Pandurangappa, M.; Lawrence, N. S.; Jiang, L.; Jones, T. G.; Compton, R. G., A sensitive reagentless pH probe with a ca. 120 mV/pH unit response. *Journal of Solid State Electrochemistry* **2004**, *8* (10), 718-721.
55. Sarapuu, A.; Helstein, K.; Vaik, K.; Schiffrin, D. J.; Tammeveski, K., Electrocatalysis of oxygen reduction by quinones adsorbed on highly oriented pyrolytic graphite electrodes. *Electrochimica Acta* **2010**, *55* (22), 6376-6382.
56. Kahlert, H., Functionalized carbon electrodes for pH determination. *Journal of Solid State Electrochemistry* **2008**, *12* (10), 1255-1266.
57. Say Hwa Tan, N.-T. N., Yong Chin Chua, Tae Goo Kang, Oxygen plasma treatment for reducing hydrophobicity of a sealed polydimethylsiloxane microchannel. *Biomicrofluidics* **2010**, *4* (3), 032204.
58. Jang, K.-J.; Suh, K.-Y., A multi-layer microfluidic device for efficient culture and analysis of renal tubular cells. *Lab on a Chip* **2010**, *10* (1), 36-42.
59. Evans, J. F.; Kuwana, T., Radiofrequency oxygen plasma treatment of pyrolytic graphite electrode surfaces. *Analytical Chemistry* **1977**, *49* (11), 1632-1635.
60. Momma, T.; Liu, X.; Osaka, T.; Ushio, Y.; Sawada, Y., Electrochemical modification of active carbon fiber electrode and its application to double-layer capacitor. *Journal of Power Sources* **1996**, *60* (2), 249-253.
61. Motin, M.; Uddin, M.; Dhar, P. K.; Mia, M.; Hashem, M., Study of Electrochemical Oxidation of Catechol in the Presence of Sulfanilic Acid at Different pH. *Portugaliae Electrochimica Acta* **2017**, *35* (2), 103-116.
62. Marsh, P. D., Dental plaque as a biofilm: the significance of pH in health and caries. *Compendium of continuing education in dentistry (Jamesburg, NJ: 1995)* **2009**, *30* (2).